Journal Name

ARTICLE

Recent Progress and Perspective in Solution-Processed Interfacial Materials for Efficient and Stable Polymer and Organometal Perovskite Solar Cells

Chu-Chen Chueh,[a] Chang-Zhi Li,[a] and Alex K.-Y. Jen[*ab]

In this review, we summarize the latest developments in solution-processed interfacial layers that have contributed to the significantly improved performance of polymer and perovskite solar cells (PSCs and PVSCs). The solution-processed interfacial materials, including organic electrolytes, organic-inorganic hybrids, graphene oxides (GOs), transition metal oxides (TMOs), and self-assembled functional materials, along with their integration into efficient PSCs, polymer tandem cells (PTCs), and the emerging perovskite solar cells (PVSCs) are discussed. Regarding the rapid progress of PSCs and PVSCs, strategies and perspectives of further improving solution-processed interfacial materials are also discussed to help readers understand the challenges and opportunities in transitioning from scientific curiosity into technology translation for realizing low-cost, printable, and high-efficiency flexible solar cells to address the scalability issues facing solar energy.

1. Introduction

Interfacial engineering has been identified as an essential approach for maximizing power conversion efficiency (PCE) of polymer solar cells (PSCs).[1-11] The typical device configuration of a bulk-heterojunction (BHJ) PSC comprises an organic photoactive layer sandwiched between two charge-collecting electrodes. In such an architecture, there are two kinds of interfaces that dominate the device performance. One is the donor-acceptor (D-A) interface within the photoactive layer that usually consists of a conjugated polymer as electron donor (D) and a fullerene derivative as electron acceptor (A). In principle, the excitons (electron-hole pair) generated in the photoactive layer need to dissociate into holes and electrons for charge extraction. However, owing to the short exciton diffusion lengths (~10 nm) and lifetimes (~10 ns) of organic semiconductors,[12-14] proper BHJ morphology with sophisticated interpenetrating networks are required to assure efficient exciton dissociation and transport before their decay to the ground state.[15-18] More importantly, the resultant nanoscale phase-separations in the BHJ can also be closely correlated with the kinetic selectivity for the electron-hole pair, which will result in separate quasi-Fermi levels of holes ($E_{F,h}$) and electrons ($E_{F,e}$) to create the incipient photo-voltage.[19] In this regard, numerous methods such as solvent additives,[20-23] molecular compatibilizers,[24-28] or modification of interfacial

dipoles[29,30] have been developed to modulate the D-A interfaces and BHJ morphology to mitigate the charge recombination loss for achieving high-performance PSCs.[31,32]

The other important interfaces of such stratified devices are the BHJ/electrode (or organic/electrode) interfaces.[3-10,33-37] In theory, after the exciton dissociation, holes will be collected at the anode while electrons will be extracted at the cathode due to the built-in electrical field created by the distinct work functions (WF) of the asymmetric electrodes in addition to the mentioned kinetic selectivity in the BHJ. Consequently, the nature of electrical contact of these organic/electrode interfaces will significantly affect the resulting photovoltaic performance including open-circuit voltage (V_{OC}), short-circuit current (J_{SC}), and fill factor (FF)).[8-10,34-36] It is well acknowledged that non-Ohmic contact will impede the charge-collecting efficiency of electrodes and cause undesirable charge accumulation at the organic/electrode interfaces, leading to decreased device performance. To alleviate these interfacial energy barriers (Φ_B), proper interfacial materials have been employed as additional buffer layers between the BHJ layer and the electrodes to optimize device performance.[7-9]

Another appealing advantage of interfacial materials is the possibility for them to provide orthogonal solvent processability relative to BHJ layers through proper molecular design to meet the requirement of high throughput manufacturing processes.[9,10,38] Therefore, the exploration of

novel solution-processed interfacial materials has attracted significant attention in this field to accomplish all-solution-processed multilayer devices.[39-44] Meanwhile, diverse functions of these interfacial layers have also been continually developed in addition to just improving electrical contact.[7-10, 38]

In order to grasp the essence of the rapid developing solution-processed interlayers in PSCs, we have summarized the most recent progresses made after our previous reviews.[8, 38] In this review, we first introduce the new features that have been discovered recently. Following this, we summarize several important developments related to solution-processable interfacial materials, including organic electrolytes, organic-inorganic hybrids, graphene oxides (GOs), transition metal oxides (TMOs), and self-assembled functional materials and their integration in high-performance PSCs. Inspired by the rapid progress of interfacial engineering made in PSCs, similar principles can also be applied to the newly discovered organometal perovskite solar cells (PVSCs) to accelerate their development with regard to their alike energy levels and device structures. Several representative progresses in PVSCs are finally discussed and highlighted to provide perspective on the future development of interfacial materials and engineering for improving solar cell performance.

2. Comprehensive Roles of Interfacial Layers in Polymer Solar Cells

In this section, we will briefly discuss the roles of interfacial materials in PSCs and introduce the new features found in recent years that can be used to enhance device processing and performance.

2.1 Energy level tuning at the organic/electrode interface

Having proper energy level alignment at the organic/electrode interface has been credited for achieving simultaneously enhanced charge collection efficiency and V_{OC} of devices.[33-36] As depicted in our previous review,[8] the intrinsic V_{OC} of BHJ PSC is determined by the energy difference between $E_{F,h}$ and $E_{F,e}$ under illumination (**Fig. 1a**).[36, 45] To achieve maximum V_{OC}, barrier-less contact (Ohmic contact) with electrodes is required, since Schottky barrier formed at either electrode will create potential loss and lower the resultant V_{OC} (**Fig. 1a, left**).[8, 38, 45] To address this issue, interfacial materials are applied to pin the electrodes' Fermi-levels to the $E_{F,h}/E_{F,e}$ of BHJ layers under illumination (**Fig. 1a, right**).[46-50]

However, energy level alignment and interfacial electronic structures at the organic/metal interfaces (BHJ layers and electrodes, herein) are quite complicated.[51] As illustrated in **Fig. 1b-c,** numerous interfacial effects have been documented. They affect the formation of interfacial dipoles to result in different degrees of vacuum-level shifting.[51, 52] Thus far, numerous studies have been dedicated to understanding the underlying mechanisms of WF tuning by interfacial materials at the organic/electrode interfaces in PSCs.[52-56] For example, Kippelen *et al.* have demonstrated that the WF modification (ΔWF) of electrodes can be achieved by simply adhering a metal or an ITO electrode to an ultra-thin (<10 nm) layer of insulating ethoxylated polyethylenimine (PEIE) or branched polyethylenimine (PEI) (structures shown in Section 4.3).[57] The ΔWF originates from two contributions: i) the intrinsic molecular dipole (μ_{MD}) associated with the neutral ethylamine group aligned along the vertical direction to the substrate, and ii)
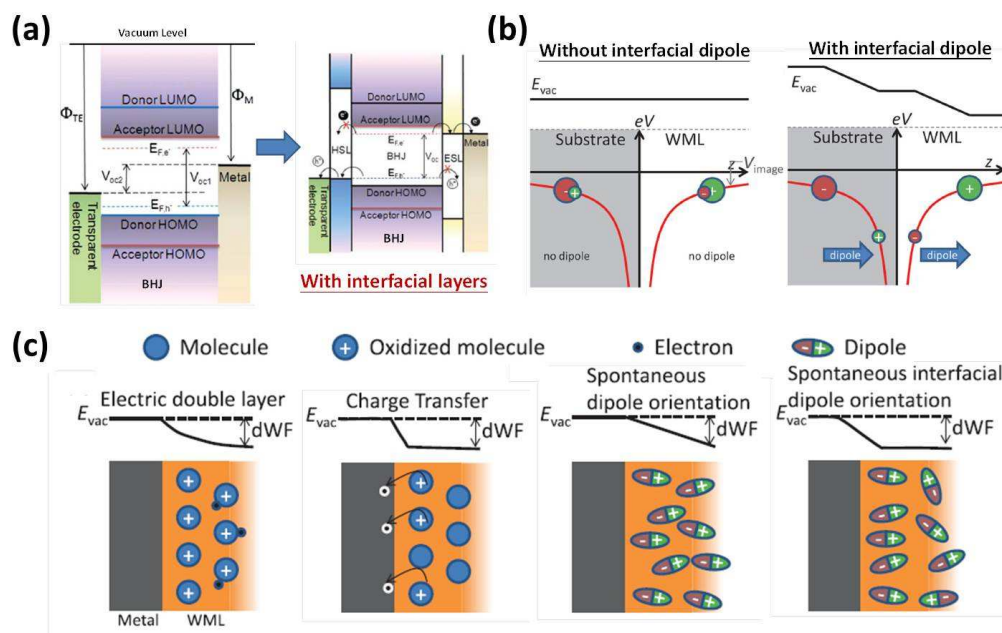
Fig. 1 (a) Energy level diagram of typical PSC without (left) and with (right) interfacial layers. Adapted with permission from ref. 8 Copyright 2012 The Royal Society of Chemistry. (b) Illustration of WF modification *via* the formation of an interfacial dipole, where the shifting of WF is indicated by E_{vac}. (c) Schematics of underlying mechanisms for WF modification by interlayer. Adapted with permission from ref. 52 Copyright 2014 Wiley-VCH Verlag GmbH & Co. KGaA.

the surface interfacial dipole (μ_{ID}) formed at the polymer/electrode interface (**Fig. 2a, left**).[58-60]

Interestingly, Lee et al. have demonstrated that the involved mechanism for ΔWF of electrodes might change if the thickness of the interfacial layer is increased. By systematically studying a series of conjugated polyelectrolytes (CPEs) with carefully controlled ion density, they revealed the importance of ionic motion and molecular reorientation in thick CPE-based interlayers (20-30 nm).[54] Basically, the formation of permanent interfacial dipoles at the electrode surface is the dominant mechanism for CPE-based interlayers to change WF and charge injection in thin-film case (<10 nm), with respect to the quantum mechanical tunnelling limit (~10 nm) (**Fig. 2a, right**).[53, 54, 61, 62] As the thickness of the interlayer exceeds such a tunnelling limit, the ionic motion or molecular reorientation within CPEs under an applied bias needs to be taken into consideration (**Fig. 2b**).[1, 63-68] In the ionic migration model, the counter ions in CPEs can independently drift to the respective electrodes under the external electrical field while the ionic side-chains of CPEs are reoriented to be adjacent to the electrodes in the molecular reorientation model. For thick CPE-based interlayers (> 20 nm), both mechanisms should have profound influences on the ΔWF and charge injection.

Importantly, Kim et al. showed that the magnitude of ΔWF derived from CPEs strongly correlates with their ionic functionalities by engineering a series of polyfluorene (PF)-based CPEs with different types of ionic groups on the side-chains.[55] As shown in **Fig. 2c**, the ionic functionalities of CPEs will result in varied dipole formations and directions at the CPE/electrode interfaces, and thereby will generate different degrees and directions of vacuum-level shifting.[54, 55, 69-72] Based on these findings, it can be concluded that the most frequently used polyelectrolytes (PEs) or compounds containing aliphatic amines basically enable the WF change of electrodes by forming net dipoles at the organic/electrode interface, leading to enhanced PSC performance, V_{OC} in particular.

2.2 Improving charge transporting and electrode selectivity

Considering the influence of interlayers on Fermi-level pinning of electrodes to the $E_{F,h}/E_{F,e}$ of BHJ layers, the device polarity and electrode selectivity can be tuned by choosing proper interfacial materials.[8, 36, 38, 73] In particular, the electrode charge selecting issue is critical for BHJ PSCs since carriers of opposite charge to the collecting electrode will be generated at the BHJ/electrode interfaces due to its D-A nanostructural texture. Consequently, additional interfacial layers with appropriate energy levels are introduced to enhance the charge selectivity of corresponding electrodes by preventing unfavorable charge recombination or exciton quenching at the organic/electrode interfaces to improve FF and the rectification of the device characteristics.

According to the type of extracted charges, the interfacial
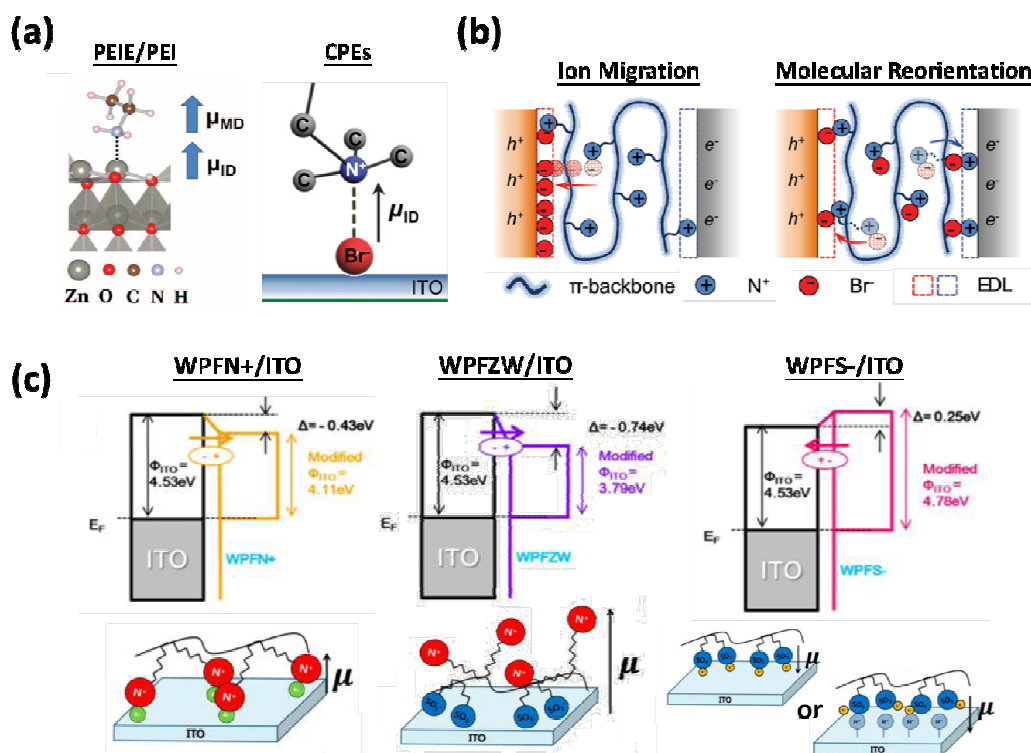
Fig. 2 (a) Molecular dipole (MD)-induced or surface interfacial diploe (ID)-induced WF change by (left) PEI/PEIE and (right) CPEs. Adapted with permission from ref. 57 Copyright 2012 AAAS and from ref. 54 Copyright 2013 Wiley-VCH Verlag GmbH & Co. KGaA. (b) Schematics of the working mechanism of thick CPEs (> 20 nm) under bias. Adapted with permission from ref. 54 Copyright 2013 Wiley-VCH Verlag GmbH & Co. KGaA. (c) Energy diagram of the CPE/ITO interfaces along with the possible of dipole formation. Adapted with permission from ref. 55 Copyright 2014 American Chemical Society.

materials can be mainly classified into p-type hole extraction layers (HELs) and n-type electron extraction layers (EELs). For an ideal HEL, its HOMO level should align with the $E_{F,h}$ of BHJ layer while its LUMO level sits above the $E_{F,e}$ of BHJ layer (**Fig. 1a**). In such way, it can only collect the holes while blocking the electrons. The same principle should be applied to the ideal EEL. Regarding the sandwiched configuration of PSCs, two types of devices, the conventional structure (ITO/HEL/BHJ/EEL/electrode) and the inverted structure (ITO/EEL/BHJ/HEL/electrode) can be fabricated with reversed electrode polarity. In general, the inverted structure has better ambient stability and compatibility to all-solution roll-to-roll processing techniques due to the possibility of using a stable (high WF) metal as top electrode.[74-78]

In addition to appropriate energy levels, possessing sufficient charge-transporting capabilities (i.e. electrical conductivity) is also essential for interfacial materials. Highly-conductive interlayers can help minimize resistance of devices and improve exciton dissociation.[79, 80] Limited by low mobility, most organic-based interlayers employed so far in devices have been restricted to few nanometers in thickness, which is much thinner than their inorganic counterparts (tens of nanometers) that have higher mobility. To address the low mobility issue, doping of organic interfacial materials has been applied to improve their electrical conductivities.[81] For example, Gregg *et al.* recently have described a water-soluble perylene diimide-based Petma$^+$OH$^-$ (structure shown in Section 4.1) that can be self-doped when dehydrated. The increased intrinsic conductivity enables it to serve as an efficient and O$_2$-stable EEL in PSCs.[82]

Jen *et al.* have introduced self-doped solution-processable

Fig. 3 (a) Conducting fullerene FPI and its *in-situ* n-doping mechanism. Adapted with permission from ref. 83 Copyright 2013 Wiley-VCH Verlag GmbH & Co. KGaA. (b) Schematic diagram of the anion-induced charge-transfer (CT) and electron-transfer (ET) of anion-π complexes regarding to their relative energy levels. (c) Schematic illustration of tetrabutyl ammonium anion (TBAX)-induced AIET to PC$_{61}$BM and its implication for the possible contact doping induced by highlighted interfacial surfactants in PSCs. Adapted with permission from ref. 84 Copyright 2014 Wiley-VCH Verlag GmbH & Co. KGaA.

fullerenes, fulleropyrrolidinium iodides (FPIs) (**Fig. 3a** and Section 4.2) as highly efficient EELs in PSCs because of their decent conductivities and appropriate energy levels.[49, 50, 83, 84] Electron transfer between the constituent iodide and adjacent fullerene core during the film evolution induces *in-situ* doping of the FPI thin-film. The anion-π interaction means that certain π-systems, such as strong π-acidity arenes (electron-accepting abilities), can interact with the approaching anions, which serve as Lewis bases to form anion-π complexes accordingly.[85] These complexes were found to behave like D-A charge-transfer (CT) complexes, exhibiting CT or electron-transfer (ET) characteristics, where the anion acts as a donor and the π-system acts as an acceptor, as illustrated in **Fig. 3b**.[86] Notably, the advantage of such an AIET in doping is its facile solution-processability at room temperature under room light without the need to engage any harsh thermal/photo-activation process.

Based on this finding, anions of widely used ammonium-based PEs were speculated to have similar capability to dope the nearby fullerenes in a BHJ layer to create better electrical contact at the organic/electrode interfaces (**Fig. 3c**).[49, 50, 83, 84] All these results highlight the importance of having proper doping in interfacial materials to enhance their charge-transporting properties and charge-collecting efficiency.

2.3 Introducing optical effects to enhance light-trapping in devices

Owing to intrinsically low carrier mobility and short exciton diffusion length of organic absorbers,[80, 87] the thickness of derived organic BHJ layers is generally restricted to 100-200 nm in order to avoid severe charge recombination loss accompanied with thicker films.[88-90] Such thin films will suffer significant optical transmission dissipation and insufficient light absorption, thereby hampering the resultant J_{SC}.[91] In this regard, delicate optical management is utilized to enhance the light absorption of photoactive layers in PSCs.[92-94] Interfacial materials also play an important role in optical engineering. For instance, a TMO-based EEL has been used as an optical spacer to alter the optical distribution within a device.[94-98] Owing to optical interference effects introduced by the interlayer, the intensity of the optical field within the photoactive layer will increase to enhance the resultant J_{SC} of devices.

Recently, utilizing the surface plasmon resonance effects derived from metallic nanostructures including light scattering, localized surface plasmon resonance (LSPR), and surface plasmon polaritons (SPPs) (**Fig. 4a**) has become a prevailing approach to enhance light-trapping of PSCs.[99-103] One of the important advantages in using this approach is that the LSPR peaks of metal nanoparticles (NPs) can be tailored through careful control of sizes and shapes to reinforce light harvesting of employed organic absorbers. In principle, utilizing the near-field effects around metal NPs can improve light harvesting of surrounding absorbers significantly and the most straightforward way is to directly incorporate NPs into the photoactive layer.[104-107] However, the direct blending of NPs
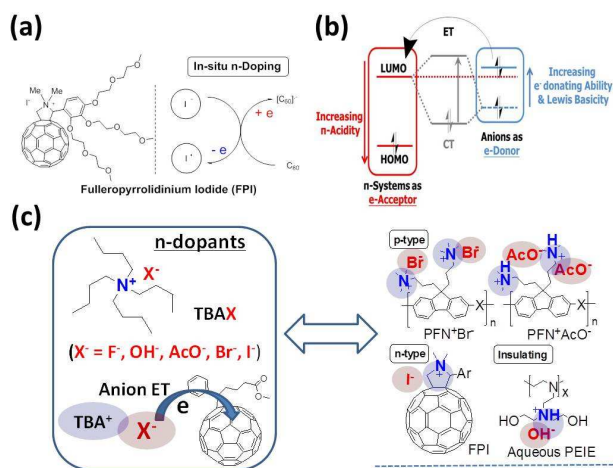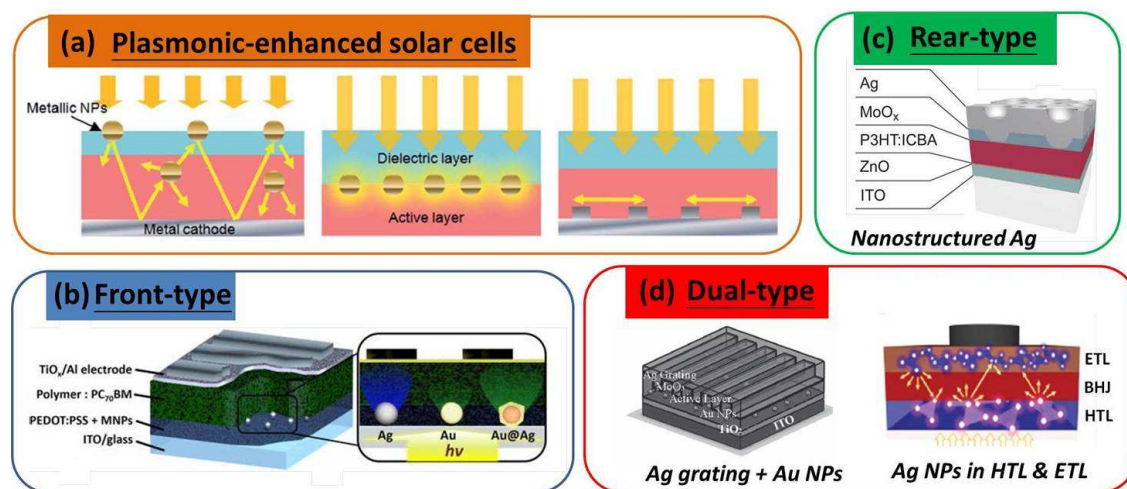
Fig. 4 (a) Structure designs of plasmonic PSCs: (Left) NP-induced light scattering; (Middle) NP-induced LSPR effects; (Right) Periodical structures-induced SPP effects. Adapted with permission from ref. 103 Copyright 2014 The Royal Society of Chemistry. (b) Front-type, (c) rear-type, and (d) dual-type plasmonic-enhanced PSCs introduced in this review. Adapted with permission from ref. 116 Copyright 2014 American Chemical Society, from ref. 119 Copyright 2013 Wiley-VCH Verlag GmbH & Co. KGaA, from 121 Copyright 2012 Wiley-VCH Verlag GmbH & Co. KGaA, and from ref. 123 Copyright 2014 Wiley-VCH Verlag GmbH & Co. KGaA.

into a photoactive layer will cause two deficiencies: i) the embedded NPs will act as recombination sites to quench excitons,[108] and ii) the incompatibility between NPs or their associated processing additives and organic absorbers will deteriorate the BHJ morphology of PSCs.[109]

For these reasons, researchers have recently pursued different routes towards plasmonic PSCs by placing metal NPs into the interlayers that can be processed through orthogonal solvent relative to the BHJ layer.[110-116] To date, the plasmonic PSCs can be divided into three types based on the position of introduced plasmonic effects in devices: front-type,[112-117] rear-type,[118-120] and dual-type[121-123] (**Fig. 4b-c**). For most front-type devices, the plasmonic effects are introduced into the charge-transporting interlayer adjacent to the light-incoming side while the rear-type devices usually consist of backside nanostructured metal electrodes. Encouragingly, the results from Yang[121] and Jen[122, 123] have described the dual-type devices by coupling metal NPs with either backside metal grating electrodes or simultaneously embedding metal NPs into dual (hole and electron) charge-transporting interlayers (**Fig. 4d**).

Another pivotal function of interlayers is that they can serve as efficient seeding layers for growing ultra-thin metal films (UTMFs) with high conductivity and transmittance.[124-126] For example, the conductivity of Ag will decrease dramatically if the Ag film thickness is below its percolation threshold (~10 nm) to result in island-like inhomogeneous morphology.[127, 128] However, this issue can be addressed by inserting a proper seeding layer to improve compatibility with ultra-thin Ag to promote the thin-film growth.[128] As a result, a UTMF with high transmittance and conductivity can be achieved to enable the development of semi-transparent PSCs[129-132] and ITO-free flexible PSCs.[124-126] Owing to the high conductivity and transmittance, such a UTMF can be employed as semi-transparent electrodes for PSCs and used to fabricate ITO-free microcavity structures for enhancing light-trapping of devices.

A state-of-the-art parallel tandem PSC with high PCE of 9.20% has been demonstrated recently by employing a UTMF as the intermediate electrode to take advantage of both semi-transparent OPV and UTMF enabled microcavity light-trapping effect.[133] All these results revealed the importance of interfacial interlayers in optical engineering for high-performance PSCs.

2.4 Modulating BHJ morphology evolution and enhancing device stability

As mentioned in our previous review, surface energy of the interlayers plays an important role in affecting the morphological evolution atop BHJ as well as its vertical phase separation,[8, 134, 135] which significantly influences the resultant charge dissociation/transport in devices. There is also an important correlation between the kinetic selectivity of an electron-hole pair and the phase-separation in the BHJ.[19, 90, 136] Hence, proper choice of interfacial materials can improve compatibility and optimize the atop-BHJ morphology. Very recently, several groups have demonstrated that the BHJ morphology could be optimized *via* rational molecular engineering of the underlying interlayers. Fang *et al.* have revealed the influence of the conjugated backbone of underlying interfacial materials on BHJ morphological evolution by comparing FBF-N and FTBTF-N EELs (structures shown in section 4.1). The latter one has two additional thiophene units on the backbone.[137] Due to the more hydrophobic nature of FTBTF-N, improved BHJ morphology is obtained, leading to improved J_{SC} and FF of the derived devices. Meanwhile, Yang *et al.* have demonstrated the importance of side-chains on underlying interfacial materials for promoting bi-continuous BHJ nanostructures. PCDTBTPho, bearing a polar phosphonate moiety on its side-chains, can serve as an efficient underlying HEL to improve the BHJ morphology of PCDTBT due to its more compatible surface energy, which not

only induces the accumulation of PCDTBT at the anode side but also helps PCDTBT to crystallize.[138]

Improving device stability is another important function of interfacial layers.[8, 139] Previously, interfacial layers have been introduced to improve adhesion between the photoactive layers and the electrodes and to enhance the durability and stability of devices, particularly for flexible PSCs.[140-142] In addition, the interlayer can also serve as an additional protecting layer for the BHJ to impede the permeation of oxygen and water. At present, poly(ethylene glycol) (PEG) derivatives are the most widely used functional materials. Usually, PEG derivatives are blended into photoactive layers to form *in-situ* self-organized PEG-based interlayers during the BHJ morphological evolution because they tend to migrate to the surface spontaneously.[143-148] These results show that the combination of proper interfacial engineering and encapsulation will enhance long-term stability of PSCs.

3. P-Type Interfacial Layers in PSCs

In this section, the modern design concepts of p-type interfacial materials and their applications in PSCs will be discussed. Note that the chemical structures of constituent conjugated polymer donors and fullerene acceptors for the discussed BHJ representatives have been extensively introduced in literature and can be easily found in other review articles[8-10, 149-151] Therefore, we will mainly focus on presenting the chemical structures of newly designed interfacial materials.

3.1 Polyelectrolytes (PEs)

Conductive PEDOT:PSS is the most commonly used solution-processed p-type interlayer in optoelectronic devices. The high conductivity of PEDOT:PSS stems from the formation of PEDOT$^+$:PSS$^-$ as a result of the efficient p-doing of PEDOT by PSSH. Based on this principle, Heeger and Bazan *et al.* have recently introduced a conductive narrow-band-gap anionic CPE (CPE-K, **Fig. 5a**) showing facile self-doped property and great potential for PSCs.[152, 153] CPE-K possesses several appealing advantages comparable to PEDOT:PSS such as orthogonal solvent processability, a suitable energy level for hole extraction (HOMO for CPE-K and PEDOT:PSS-4083: 4.9 and 5.0 eV), reasonably high electrical conductivity (for CPE-K and PEDOT:PSS-4083: 1.5 x 10^{-3} and 2.7 x 10^{-3} S/cm), and decent optical transparency.[152] Moreover, CPE-K has a neutral pH value around 7.56, which greatly alleviates the concern for the acidic nature of PEDOT:PSS (PH: 1-2). As a result, a PTB7:PC$_{71}$BM device using CPE-K HEL showed a high PCE of 8.2% (V_{OC}: 0.71 V; J_{SC}: 16.29 mA/cm^2; FF: 0.69), surpassing that of the control PEDOT:PSS device (7.9%). The main reason for enhanced device performance lies on improved FF, which is attributed to reduced bulk resistance because of highly conductive CPE-K and modified HEL/BHJ interface.[152]

Bazan further unveiled the doping mechanism of CPE-K[153] that involves the initial double protonation of single polymer backbone. In addition, the pendant sulfonate groups function to stabilize the formed cationic polarons (radical cations) through the Coulombic interaction. Two additional CPEs, PCPDTPhSO$_3$Na and PFBTSO$_3$Na (**Fig. 5a**) were juxtaposed to clarify the influence of the constituent moieties in CPE-K on the resulting self-doped property. Interestingly, PCPDTPhSO$_3$Na showed a clear polaron absorption with broad transition extending to 1000 nm after dialysis while PFBTSO$_3$Na did not exhibit such absorption. The loss of self-doping property in PFBTSO$_3$Na clearly elucidates the importance of CPDT units on p-doping phenomenon. This might be because the electron-rich CPDT moiety contributes to a relatively high-lying HOMO in the derived polymer to facilitate doping during dialysis.[153]
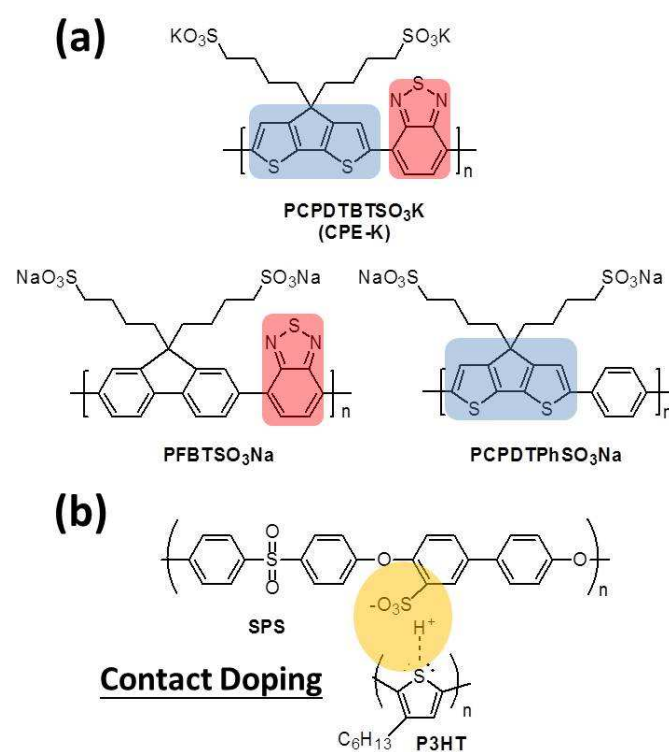
Fig. 5 (a) Structures of the introduced narrow-E$_g$ anionic CPEs. Adapted with permission from ref. 153 Copyright 2014 Wiley-VCH Verlag GmbH & Co. KGaA. (b) Illustration of the contact doping between the sulfonic acid groups of SPS and P3HT. Adapted with permission from ref. 155 Copyright 2014 Wiley-VCH Verlag GmbH & Co. KGaA.

In addition to the development of intrinsically conductive CPE-based HELs,[154] contact doping at the organic/electrode interface can also improve the electrical contact of electrodes as aforementioned. A sulfonated poly(phenylsulfone) (SPS, **Fig. 5b**) HEL was recently reported by Gomez *et al.* that functioned as efficiently as PEDOT:PSS in PSCs.[155] SPS localized at the anodic interface acts like a strong polymeric acid, creating interfacial doping of polymer in BHJ. Such contact doping can effectively alleviate the interfacial Φ_B to facilitate charge

collection. However, limited by the insulating nature of SPS, the enhanced performance is greatly dependent on the degree of sulfonation on SPS and its thickness (< 3 nm). All these findings show the great potential of using organic PEs as advanced HELs in PSCs.

3.2 Graphene oxides (GOs)

Due to their unique two-dimensional structures and easily tailorable electronic properties, solution-processable GO-based interlayers have also attracted significant attention recently as useful interlayer materials.[156, 157] GO HEL was first introduced by Chen *et al.* in 2010 for PSCs.[158] The WF of GO (-4.7 eV) was evaluated for its suitability to function as a HEL that can be processed into uniform film on ITO anode. Meanwhile, the carboxylic acid and phenolic/enolic groups on GO were found by Jen *et al.* to effectively dope conjugated polymers (in BHJ) through protonic doping to result in highly efficient PSCs.[159]

Fig. 6 (a) GO HEL-induced preferential face-on PTB7 π-stacking and enhanced stability of the derived device. Adapted with permission from ref. 165 Copyright 2011 American Chemical Society. (b) Synthetic route of GO-OSO$_3$H. Adapted with permission from ref. 167 Copyright 2012 American Chemical Society. (c) Synthetic route of GOR by oxidative unzipping of SWCNTs and the related energy level diagram of the derived device. Adapted with permission from ref. 170 Copyright 2014 Wiley-VCH Verlag GmbH & Co. KGaA.
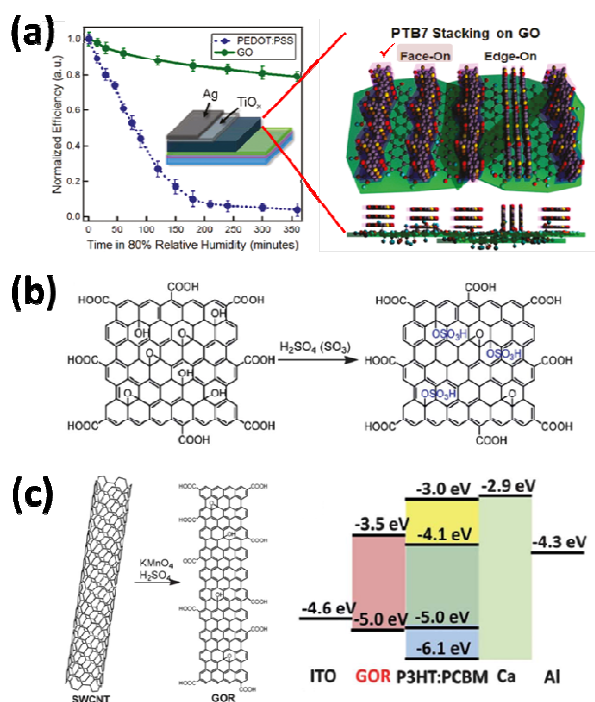
However, the insulating nature of GO limits its thickness to be ~ 2 nm for use in devices, which significantly impedes GO's use in practical applications.[160] In this regard, various chemical or thermal reduction strategies have been introduced to convert GO back to its pristine conjugated structure to enhance electrical conductivity.[161] Such reduced GO (r-GO) is

considered to have better charge extraction ability compared to GO. Nevertheless, the r-GOs generally have decreased solubility in common organic solvents compared to GO, which inevitably creates problems with poor film formation and surface coverage on substrates. In this regard, versatile approaches have been exploited recently to improve the solution processibility of r-GO or conductivity of GO-based films.

Post-thermal annealing of GO HEL is a very simple method to get r-GO to enhance device performance since the pristine oxygen-containing groups can be removed by eliminating H$_2$O, CO$_2$, etc. during annealing at temperatures between 230 and 250 $^{\circ}$C.[162, 163] The thermal reduction of GO is evident in the decreased density of C-O, C=O, and CO$_2$H in X-ray photoelectron (XPS) spectra and the increased conductivities. Meanwhile, Li *et al.* have delineated that chemically modified GO HEL by O$_2$ plasma post-treatment afford a better device performance (30% enhancement) than using GO as HEL due to its higher WF (-5.2 eV) than GO (-5.0 eV). The higher WF results from more surface C=O dipoles generated by extracting electrons from graphene.[164] On the other hand, Hersam's group showed that the UV-ozone (UVO) post-treatment of GO HEL can modulate the BHJ morphology.[165] As shown in **Fig. 6a**, the UVO-treated GO can promote preferential face-on π-stacking atop PTB7 to facilitate vertical charge transport/extraction in PSCs. Consequently, it enabled the high PCE (7.39%) of the derived PTB7:P$_{71}$BM device with outstanding thermal/ambient stability compared to those derived from PEDOT:PSS.

Recently, reduced GO with specific chemical reagents has been reported by several groups. For example, a new solution processable r-GO (pr-GO) HEL with much improved film formation *via* spin-coating has been developed by Na *et al.* by introducing *p*-toluenesulfonyl hydrazide (*p*-TosNHNH$_2$) into precursor solution.[166] The derived P3HT:PC$_{61}$BM device showed an improved PCE of 3.63% compared to those using GO or conventional r-GO. Soon after, a solution processable sulfated GO was described by Dai *et al.* (GO-OSO$_3$H, **Fig. 6b**), in which the GO was reduced by dehydrating with fuming sulfuric acid.[167] Due to attached -OSO$_3$H groups along with the original –COOH groups in GO, GO-OSO$_3$H has much improved solution processability. In addition, it possesses a much higher conductivity (1.3 S/m *vs*. 0.004 S/m) than GO. As a result, a superior PCE (4.37%) of the derived P3HT:PC$_{61}$BM device is accomplished.

Hybridizing conductive fillers with GO is another promising way to increase its conductivity. For instance, Huang *et al.* have reported a solution processable GO:SWCNT composite HEL.[168] By blending with small diameter (~1 nm) SWCNTs, it is able to maintain the original smooth surface of the composite thin-film while greatly enhancing its vertical conductivity. Hence, such GO:SWCNT composites enable the use of thicker and easier-to-make HELs for device fabrication. Conductive PEDOT:PSS has also been blended into GO HELs for enhancing device performance. Lately, Tan *et al.* have successfully coupled plasmonic effects into GO/PEDOT:PSS hybrid HELs by blending Au NP-decorated GO (Au-GO) with

PEDOT:PSS.[169] In this case, GO is able to serve as a good template for uniform dispersion of Au NPs without causing problematic aggregation as abovementioned.

Very recently, a graphene oxide nanoribbon (GOR)-based HEL has been developed by Dai *et al.* by oxidative unzipping of SWCNTs with KMnO$_4$ in concentrated H$_2$SO$_4$ (**Fig. 6c**).[170] In such way, GOR can retain the solution processability of GO and the semiconducting properties of graphene nanoribbon. It possesses proper energy levels for hole-transporting and electron-blocking (**Fig. 6c, right**), which results in a high PCE of 4.14% in PEHT:PCBM device. It can also be used in conjunction with PEDOT:PSS or p-type TMOs to form bilayer HELs for high-performance PSCs.[171, 172]

3.3 Solution-processed transition metal oxides (TMOs)

Inorganic interlayers also have progressed rapidly in the past few years because of their superior electronic properties and respectable environmental stability compared to their organic counterparts. Among these, TMOs with decent transparency across visible and infrared spectra have been widely proven to form good Ohmic contact with organic absorbers due to their high conductivity and appropriate WF.[173, 174] In order to meet the requirements for large-scale and high-throughput production of organic electronics,[175] the recent development of TMOs has been focused on improving solution processing techniques, as depicted in **Fig. 7a**. At present, most of the TMOs are mainly synthesized *via* the sol–gel route. Such sol-gel-made TMOs usually require high-temperature post-annealing (300-600 ^{o}C) to achieve high crystallinity, which is incompatible with the high-throughput manufacturing protocols for organic photovoltaics. Moreover, although high-crystallinity TMOs have higher charge mobility than the less crystalline ones, the derived grain boundaries might result in severe trap states, which is unfavorable for device performance and stability.[175] Hence, the research focus in this field has shifted to developing low-temperature processed TMO-based interlayers, for which reasonably crystallinity can still be achieved. To date, various solution processed TMO HELs have been exploited based on different chemical routes, such as NiO$_x$,[176-179] MoO$_x$,[180-184] VO$_x$,[185-188] WO$_3$,[189-191] ReO$_x$,[192] RuO$_x$,[193] CuO$_x$,[194] CrO$_x$,[195] and Fe$_3$O$_4$.[196]

The working mechanisms of TMO HELs are quite different due to their distinct electronic structures. In general, TMOs can be divided into n-type and p-type semiconductors according to their corresponding electronic states. The n-type TMOs possess deep-lying energy levels and WF (usually exceeding 6 eV). Accordingly, the Fermi-level pinning

between a photoactive layer and a TMO HEL can be achieved by matching the LUMO level of TMOs and the HOMO level of a donor polymer in BHJ. Differently, the p-type TMOs with slightly lower WF than n-type ones accomplish the Fermi-level pinning with the HOMO level of a donor polymer in BHJ through its HOMO level while their wide E$_g$ can create an energy barrier for blocking electrons. In this regard, MoO$_x$, VO$_x$, WO$_3$, and CuO$_x$ are classified as n-type TMOs while NiO$_x$ and CrO$_x$ are considered as p-type. Also, it must be noted that the WF of TMOs is also strongly correlated with their deposition methods, surface characteristics, and crystal structures.[173, 175, 197]

Recent advances of n-type TMO HELs are introduced herein. For MoO$_x$, a facile and low-cost method has been introduced by Yang *et al.* to prepare a low-temperature (80 ^{o}C)-processed MoO$_3$ HEL from aqueous solution of the (NH$_4$)$_6$Mo$_7$O$_{24}$-4H$_2$O precursor.[182] Meanwhile, a post-treatment-free MoO$_x$ HEL based on a MoO$_x$ NP suspension solution has been developed by Lee *et al.* using microwave-assisted synthesis.[181] Soon after, a low-temperature-annealed (80 ^{o}C) MoO$_3$ HEL *via* a simple one-step synthesis has been reported by Chou *et al.* to fabricate a high-performance (7.75%, **Table 1**) PBDTTT-C-T:PC$_{71}$BM device, outperforming the control PEDOT:PSS device.[184] They have also successfully demonstrated that a low-temperature-annealed (100 ^{o}C) V$_2$O$_5$ HEL could result in high PCE (7.62%) as well (**Table 1**). Moreover, they revealed that excess oxygen in TMOs is
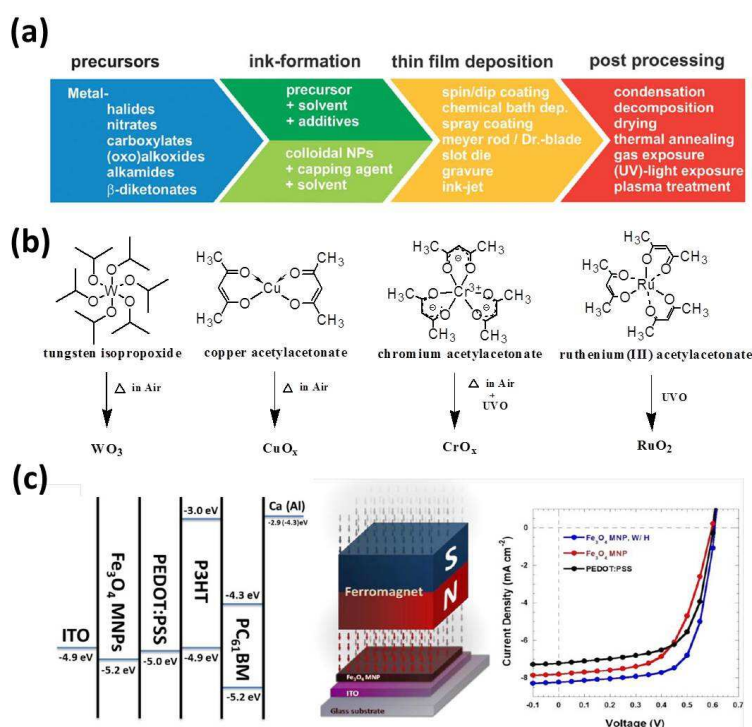
Fig. 7 (a) Solution-derived preparation of TMO-based interlayers. Reprinted with permission from ref. 175 Copyright 2013 The Royal Society of Chemistry. (b) Precursor structures and involved treatment of introduced TMO-based HELs. (c) Illustration of the fabricated Fe$_3$O$_4$ HEL device under external magnetostatic field alignment and its related energy level diagram and *J-V* characteristics. Adapted with permission from ref. 196 Copyright 2013 Wiley-VCH Verlag GmbH & Co. KGaA.

Table 1. Device Characteristics of representative PSCs using TMO-based HELs.

Device Structure	V_{OC} (V)	J_{SC} (mA/cm^2)	FF	PCE (%)	Ref.
ITO/MoO$_3$/PBDTTT-C-T:PC$_{71}$BM/Ca/Al	0.76	16.38	0.62	7.75	184
ITO/V$_2$O$_5$/PBDTTT-C-T:PC$_{71}$BM/Ca/Al	0.76	16.47	0.61	7.62	184
ITO/WO$_3$/P3HT:IC$_{70}$BA/Ca/Al	0.84	10.85	0.70	6.36	191
ITO/CuO$_x$/P3HT:IC$_{60}$BA/Ca/Al	0.87	11.08	0.70	6.72	194
ITO/NiO$_x$/pDTG-TPD:PC$_{71}$BM/LiF/Al	0.82	13.90	0.68	7.82	178
ITO/CrO$_x$/P3HT:IC$_{60}$BA/Ca/Al	0.87	10.74	0.70	6.55	195
ITO/ReO$_x$/P3HT:IC$_{60}$BA/Ca/Al	0.84	11.28	0.77	7.26	192
ITO/ReO$_x$/PBDTTT-C-T:PC$_{71}$BM/Ca/Al	0.76	17.74	0.62	8.30	192
ITO/RuO$_2$/PBDTBDD:PC$_{71}$BM/Ca/Al	0.84	12.66	0.70	7.45	193

undesirable for high device performance.[184] Recently, an ambient processable V$_2$O$_5$ HEL has been introduced Lira-Cantú *et al.* from an aqueous solution of sodium metavanadate, which formed layered V$_2$O$_5$ hydrate (V$_2$O$_5$·0.5H$_2$O) in thin-films.[188] The contained H$_2$O induces decent stability of resultant films under working conditions.

As for WO$_3$, a low-temperature (80 $^{\circ}$C)-processed WO$_3$ HEL has been developed by Barbec *et al.* without oxygen post-treatment. It works well for both conventional and inverted device structures.[189] Later, Kim *et al.* have described a facile sol-gel route from tungsten ethoxide (W(OC$_2$H$_5$)$_6$) precursor solution for an annealing-free WO$_3$ HEL.[190] Li *et al.* further showed that hole mobility of 9.4 x 10^{-3} cm^2/V·s could be achieved for WO$_3$ prepared from an analogue tungsten isopropoxide precursor (W(OC$_3$H$_7$)$_6$, **Fig. 7b**) followed by thermal annealing at 150 $^{\circ}$C in air. It led to a high PCE (6.36%, **Table 1**) in a P3HT:IC$_{70}$BA BHJ device.[191] A similar approach was employed to develop a solution-processable CuO$_x$ HEL using precursor copper acetylacetonate (Cu(acac)$_2$, **Fig. 7b**).[194] The derived P3HT:IC$_{60}$BA and PBDTTT-C:PC$_{71}$BM devices showed impressive PCEs of 6.72% and 7.14% (**Table 1**), significantly exceeding those derived from using PEDOT:PSS.

NiO$_x$ is the most widely studied p-type TMO HEL in the literature.[174-176] Recently, So *et al.* have reported a solution-derived NiO$_x$ *via* thermolysis (275 $^{\circ}$C) of the precursors of nickel acetate tetrahydrate (Ni(CH$_3$COO)$_2$·4H$_2$O) and monoethanolamine in ethanol. Such a NiO$_x$ HEL afforded a high PCE (7.82%, **Table 1**) in a pDTG-TPD:PC$_{71}$BM device.[178] Meanwhile, UVO post-treatment was utilized by Ma to further reduce the processing temperature of NiO$_x$.[177] Due to high surface concentration of NiOOH through cooperative treatments, the annealing temperature can be reduced to below 150 $^{\circ}$C. Very recently, an annealing-free NiOx HEL prepared from colloidal crystalline NiO NPs *via* sonochemical synthesis was delineated by Xie *et al.*.[179] NiO NPs with 4-8 nm in size could be obtained at low temperature through ultrasonic irradiation. Recently, Li *et al.* have demonstrated a new efficient p-type CrO$_x$ HEL[195] by spin-coating the precursor chromium acetylacetonate (Cr(acac)$_3$, **Fig. 7b**) with subsequent thermal annealing (60 $^{\circ}$C) and UVO treatment. The CrO$_x$ HEL can improve the PCE of a P3HT:IC$_{60}$BA based device from 6.06% (PEDOT:PSS-based device) to 6.55% (**Table 1**).

Based on a similar principle, Li *et al.* have also prepared two new solution-processed TMO HELs, ReO$_x$ and RuO$_2$.[192, 193] ReO$_x$ HEL is prepared by depositing the methyltrioxorhenium (VII) (CH$_3$ReO$_3$, i.e. MTO) precursor followed by post annealing (110 $^{\circ}$C) in air, in which MTO was gradually converted into organometallic oxide polymeric MTO ([CH$_3$ReO$_3$] $_\infty$, i.e. poly-MTO) as a result of reacting with moisture.[192] Afterward, UVO treatment in air is conducted to decompose this into the final ReO$_x$. Notably, such ReO$_x$ can enhance the optical distribution in BHJ layers due to the better-matched refractive index. This ReO$_x$ HEL can result in high-performance P3HT:IC$_{60}$BA (7.26%) and PBDTTT-C-T:PC$_{71}$BM devices (8.30%) (**Table 1**), where a 14% PCE enhancement could be achieved compared to PEDOT:PSS-based device. A RuO$_2$ HEL can be obtained by direct UVO treatment of the spin-cast films of ruthenium(III) acetylacetonate (Ru(acac)$_3$ precursor, **Fig. 7b**) without annealing.[193] The RuO$_2$ HEL enables the PBDTBDD:PC$_{71}$BM BHJ device to achieve higher PCE of 7.45% (**Table 1**) than that of the PEDOT:PSS derived device. On the other hand, Gong *et al.* have recently introduced solution processed Fe$_3$O$_4$ magnetic NPs as HEL. Owing to their magnetic properties, an applied external magnetostatic field can be used to align the Fe$_3$O$_4$-based thin-film, leading to enhanced conductivity and device performance, as illustrated in **Fig. 7c**.[196]

4. N-Type Interfacial Layers in PSCs

Compared to their p-type counterparts, n-type interfacial materials have experienced even more prosperous growth in PSCs in the past few years.[9, 10] In the following sections, we will summarize the latest development of EELs including their molecular structures and applications in PSCs. With regard to the distinct nature and structures of newly developed n-type interfacial materials, we will categorize them into seven subsections for individual discussion. A more detailed introduction can be found in recent review articles.[9, 10]

4.1 Non-fullerene oligomers

Shown in **Fig. 8** are the non-fullerene oligomer-based EELs developed lately. They can be divided into three main categories, including non-conjugated oligomers (DCDA and Urea),[198] perylene-diimide (PDI)-based salts ((PTCDI$^+$)I$^-$,[199] Petma$^+$OH$^-$,[82] and PDINO[200]), and other polycyclic aromatic compounds (Rhodamine 101,[201] F8PS,[202] 3TPA-FEP,[203] and FTBTF-N[137]).

The amino-containing (-NH$_2$) non-conjugated oligomers, DCDA and Urea, have been recently introduced by Yang *et al.*.[198] They revealed that the -NH$_2$ group could coordinate with
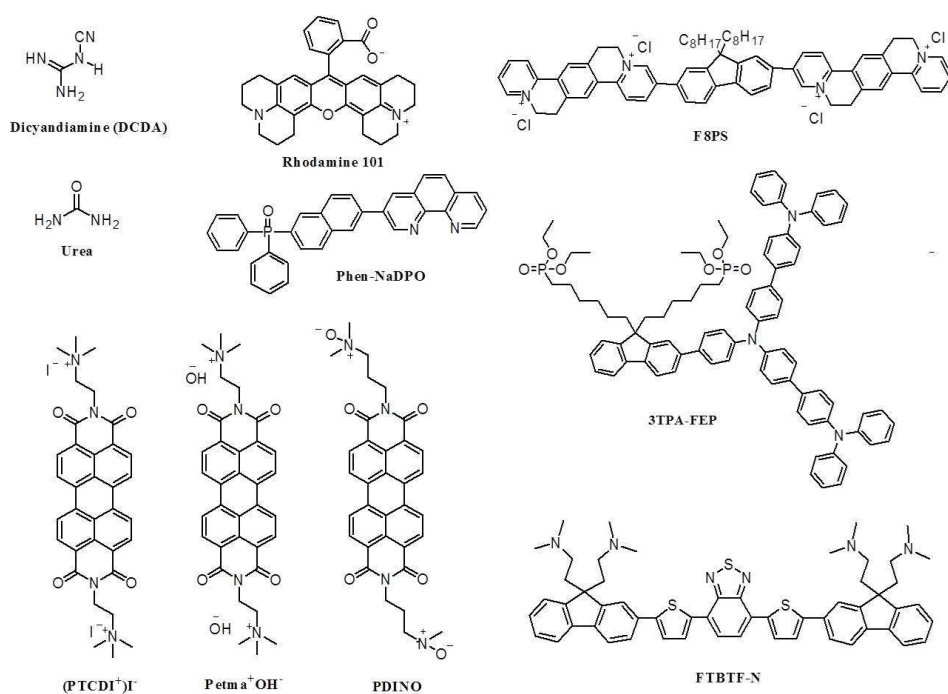
Fig. 8 Recently developed non-fullerene oligomer-based materials as EELs in PSCs.

Al atoms to prevent undesirable interactions at P3HT/Al interface. Besides, the density of amino groups in oligomers affected the interfacial dipole formation at BHJ/Al interface to result in a different degree of WF shifting of Al. Consequently, different degrees of PCE enhancement in devices (~27% for DCDA and ~31% for Urea) were observed.

The PDI salt-based HELs are other attractive candidates for high-efficiency PSCs due to their extended planar structures for electron transport. For instance, the solution-derived electrostatic layer-by-layer (eLbL) approach has been employed by Buriak *et al.* to prepare a PTCDI$^+$:PEDOT:PSS$^-$ composite EEL from (PTCDI$^+$)I$^-$ and PEDOT:PSS to tune ITO WF.[199] Meanwhile, a self-doped Petma$^+$OH$^-$ EEL with decent conductivity has also been reported by Gregg *et al.*, as discussed in Section 2.2.[82] Very recently, an environmentally stable and thickness-insensitive PDINO EEL has been reported by Li *et al.*.[200] Due to self-organized π-stacking of PDI units, the PDINO EEL shows an intrinsic conductivity of ~10^{-5} S/cm, and thus can be operated in a wide thickness range (6-25 nm). By combining this with its WF tuning ability from the ionic feature, the PDINO EEL can be used to induce high PCE (8.35%) in a PTB7-Th:PC$_{71}$BM BHJ device (**Table 2**).

For other polycyclic aromatic compounds, a conjugated zwitterion Rhodamine 101 EEL has been developed by Ouyang *et al.*. The zwitterionic moiety can form a strong dipole at the BHJ/electrode interface to improve the resulting device performance.[201] Meanwhile, Su *et al.* have reported an alcohol-soluble pyridinium salt, F8PS, comprising positively charged pyridinium rings and halide counterions to function as an efficient EEL in PSCs.[202] An alcohol-soluble star-like 3TPA-FEP EEL consisting of a triphenylamine (TPA) core featuring TPA/phosphonate side-chains (FEP) was subsequently

described[203] with polar FEP groups that could form interfacial dipoles at the BHJ/electrode interface.[204] By using a 3TPA-FEP EEL, the PCE of PCDTBT:PC$_{71}$BM device was further improved to 7.21% (**Table 2**). In addition, FTBTF-N has also been reported recently by Fang *et al.* as discussed in Section 2.4. It can serve as an underlying EEL to modulate the atop-BHJ morphology, thereby enhancing the PCE of a benchmark PTB7:PC$_{71}$BM device to a very high PCE of 9.22% (**Table 2**).[137]

4.2 Fullerene derivatives

Due to similar energy levels and structures as PCBMs, the development of water/alcohol soluble fullerene derivatives as EELs has also attracted wide attention. The representative examples of newly developed fullerene-based EELs are presented in **Fig. 9**, where they can be categorized into two parts: modified C$_{60}$/C$_{70}$s (left) and fulleropyrrolidines (right).

For the modified C$_{60}$s, a series of functional fullerenes including a PEG end-caped C$_{60}$ (PEGN-C$_{60}$)[205] and a -NH$_2$ group containing C$_{60}$ (DMAPA-C$_{60}$)[206] have been developed by Li *et al.* as efficient EELs in PSCs. These functional groups (PEG and -NH$_2$) assist in alignment of the energy levels at the BHJ/electrode interface and result in subtle dependence of V_{OC}s on employed electrodes. Accordingly, high PCEs could be achieved in PBDTTT-C-T:PC$_{71}$BM devices using PEGN-C$_{60}$ (7.45%) and DMAPA-C$_{60}$ (7.42%) EELs (**Table 2**). They also reported an efficient PCBDAN EEL that was synthesized by modifying the ester groups of PC$_{61}$BM with amine end-groups.[207] Besides, by simple methylation of PCBDAN with methyl iodide, the derived salt, PCBDANI (**Fig. 9**), could be prepared. Owning to their polar side-chains, both alcohol-soluble PCBDAN and PCBDANI can form interfacial dipoles at the BHJ/electrode interface. Consequently, an even higher PCE of 7.69% was demonstrated (**Table 2**).

Notably, self-doping of PCBDANI was evident from electron paramagnetic resonance measurements and from the high intrinsic conductivity (1.98x10^{-2} S/cm). This enables PCBDANI EEL to function effectively even at thicker layer (82 nm).[208] Meanwhile, Huang and Cao *et al.* described a PC$_{71}$BM-N EEL (**Fig. 9**) by functionalizing PC$_{71}$BM with a tertiary amino group.[209] In addition to WF tuning, PC$_{71}$BM-N EEL induces contact doping at the BHJ/electrode interface by forming intermediate amine:C$_{70}$ complexes. Similar synthetic routes have also been employed to prepare a B-PCPO EEL (**Fig.**
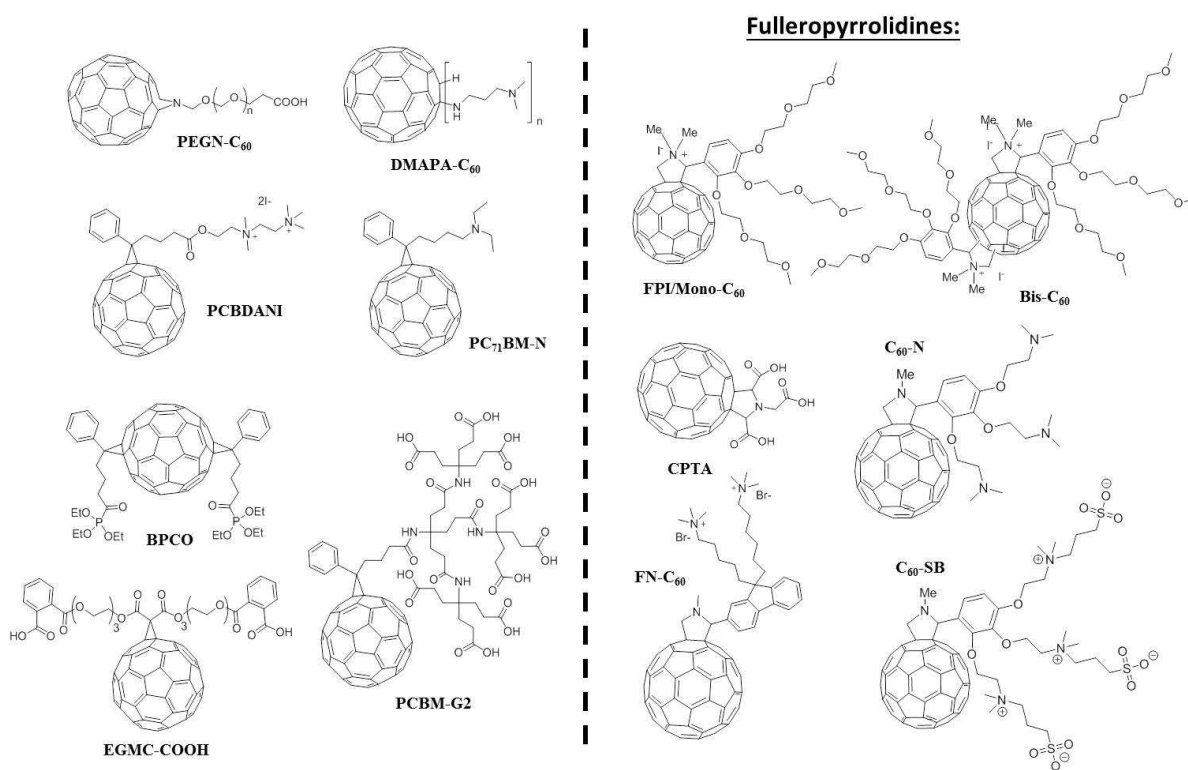
Fig. 9 Recently developed fullerene-based materials as EELs in PSCs.

9).[210] Due to the polar phosphate side-chains, B-PCPO showed reasonable alcohol processability and tuning of ITO WF, thereby leading to improved performance in PCDTBT:PC$_{71}$BM based devices.

An alcohol soluble EGMC-CO$_2$H EEL has been recently prepared by Cheng and Hsu *et al.* (**Fig. 9**) by decorating C$_{60}$ with hydrophilic triethylene glycol (TEG) functional groups.[211] This EGMC-CO$_2$H EEL can react with alkali carbonates to enhance its electron-transporting properties. Doping might stem from the ionic EGMC-carboxylate salts formed by interacting -CO$_2$H groups with carbonate bases. Lately, Gong *et al.* have reported a conductive PCBM-G2 EEL (**Fig. 9**) by modifying PC$_{61}$BM with an amine dendron.[212] Due to its pH neutrality, no interfacial dipoles are formed at the interface, but the conductive PCBM-G2 can reengineer the surface electronic characteristics of ZnO, leading to a 30% enhancement in PCE with largely improved J_{SC} and FF.

Recently, fulleropyrrolidines-based EELs (**Fig. 9, right**) have also been extensively studied. As discussed in Section 2.2, two excellent cathode-independent FPI-based EELs, Mono-C$_{60}$ and Bis-C$_{60}$, have been introduced by Jen *et al.* for achieving high-efficiency and stable PSCs. The success of such EELs lies in self-doping *via* AIET and the WF-tuning capability induced by the ionic features.[49, 50, 83, 84] The Bis-C$_{60}$ EEL afforded a high-performance PIDTT-DFBT:PC$_{71}$BM device (7.66%, **Table 2**) which can be further enhanced to over 9% by coupling with plasmonic enhanced light absorption into the HEL and EEL.[123] Shortly after, Bo *et al.* described a FN-C$_{60}$ EEL, which was synthesized from C$_{60}$ and aldehyde fluorene

via the Prato reaction.[213] Meanwhile, Fang *et al.* reported the use of a commercially-available C$_{60}$ pyrrolidine tris-acid (CPTA) as an EEL to improve the PCE of PTB7:PC$_{71}$BM from 4.83% to 7.92%.[214] Very recently, two amine (C$_{60}$-N) and sulfobetaine (C$_{60}$-SB)-substituted fulleropyrrolidines have been introduced by Russell and Emrick *et al.* as excellent cathode-independent EELs in PSCs.[215] Variable thicknesses of such fulleropyrrolidines-based EELs were engineered to investigate possible underlying mechanisms and the degree of shifting electrode WF. The ΔWF of electrodes was proposed to be mainly caused by the permanent dipole formed at the BHJ/electrode interface *via* the zwitterionic C$_{60}$-SB while the WF changes of electrodes were due to induced charge transfer of C$_{60}$-N. Finally, high-performance PTB7-Th:PC$_{71}$BM devices with high FFs and much improved ambient stability could be achieved by using C$_{60}$-SB (8.57%) and C$_{60}$-N (9.35%) EELs compared to the control Ca/Al devices. More recently, an excellent fullerene-based EEL composite consisting of conductive FPI (Bis-OMe) and small amount of insulating PEIE has been introduced by Jen *et al.*.[216] Inheriting the self-doping property from Bis-OMe, such a hybrid EEL possesses improved conductivity and can dope the PCBMs in BHJ through contact in addition to tuning the WF of electrode, enabling this composite EEL to function well in thicker film (~50 nm). As a result, a high PCE of 9.62% could be achieved in the inverted PTB7-Th:PC$_{71}$BM device (**Table 2**). All these results affirm the great potential of using fulleropyrrolidines-based EELs for achieving high-efficiency PSCs.
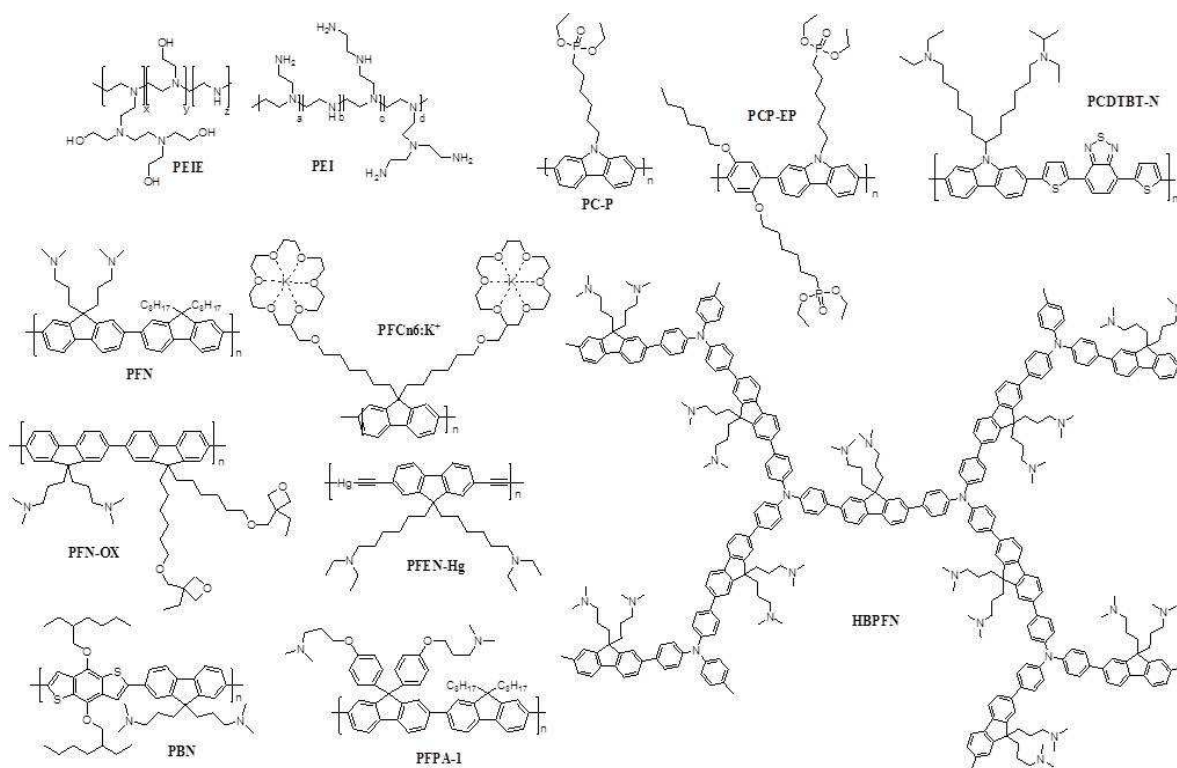
Fig. 10 Recently developed neutral EELs based on neutral polymers.

4.3 Neutral polymers

There are three main types of n-type neutral polymer interlayers as summarized in **Fig. 10** including PEIE/PEI, PFN-based and polycarbazole (PC)-based derivatives. Most of these neutral compounds are soluble in alcohol with the assistance of a small amount of acetic acid (AcOH).

As discussed in Section 2.1, PEIE/PEI have been widely used in PSCs including in single junction and tandem cells (Section 6) after the work of Kipplen *et al.*[57] Based on this discovery, Kim *et al.* utilized PEI to facilitate pinning the energy level of ZnO/BHJ interface to improve the performance of PTB7:PC_{71}BM device from 6.99% (ZnO device) to 8.76% (ZnO/PEI device, **Table 2**) because PEI can form interfacial dipoles on ZnO surface and reduce its roughness simultaneously.[217]

PFN-based EELs are another popular class of materials for high-efficiency PSCs.[218] It has been shown by Wu *et al.* that PFN could modify the WF of ITO to promote Ohmic contact at the ITO/BHJ interface, thereby increasing the PCE of the PTB7:PC_{71}BM device to 9.21% (**Table 2**). Later, a $PFCn6:K^+$ EEL was synthesized by Chen *et al.* which has a metal-ion-intercalated crown ether grafted on the PF conjugated polymer backbone.[219] It enabled a record high PCE (7.5%, **Table 2**) to be realized in a P3HT-based BHJ due to enhanced electron extraction and optical enhancement. Afterward, an amino-containing conjugated metallopolymer PFEN-Hg EEL with Hg incorporated in the polymer backbone has been shown by

Huang and co-workers to possess improved charge-transporting properties.[220] It not only helped realize high performance (9.11%, **Table 2**) in PTB7:PC_{71}BM device but also provided a broader range of film thickness (7-20 nm) for device fabrication than that for PFN-OX EEL (<5 nm).

Despite the thickness issue, PFN-OX EEL can be crosslinked to possess superior solvent resistance. It also facilitated high PCE (9.13%) device to be realized for another BHJ system (PBDTTT-C-T:PC_{71}BM).[221] Moreover, it can be used to modify ZnO EEL to enhance efficiency of the PTB7:PC_{71}BM device from 8.45% (ZnO device) to 9.28% (ZnO/PFN-OX device) with an extremely high FF (0.74) due to doping of PCBM by PFN-OX.[222] Recently, Park *et al.* have developed a conjugated PBN EEL, comprising benzodithiophene (BDT) and fluorene moieties, to modify ZnO.[223] PBN can create interfacial dipoles at the ZnO/BHJ interface and improve physical contact between BHJ and ZnO due to its hydrophobic properties, thereby resulting in a 21.1% PCE improvement in the derived devices.

Recently, Li and Chen have reported a hyperbranched HBPFN EEL that helped realize a high PCE of 7.55% in a PBDTTT-C-T:PC_{71}BM BHJ device, surpassing the PCE of the device using a linear PFN EEL (6.88%).[224] Inganas' *et al.* also reported PFPA-1 EEL as a pivotal interlayer in an inverted ITO-free device that can not only effectively up-shift the WF of underlying metal cathodes but also optimize the BHJ morphology to substantially improve the device performance.[225, 226]

PC-based EELs have also been investigated recently. Chen *et al.* reported a series of PC-based EEL, PC-P and PCP-EP, by decorating PC homopolymers and copolymers with phosphonate side-chains.[227-228] Such hydrophilic side-chains can tune the ITO WF by forming interfacial dipoles and supply a sub-gap state for electron transport, leading to an improved PCE.[227] Lately, Huang *et al.* also reported an alcohol soluble PCDTBT-N EEL that was functionalized with polar amino groups.[209] The amino groups have the tendency to form amine:C_{70} complexes to facilitate electron extraction which is similar to the aforementioned $PC_{71}BM$-N case (Section 4.2).

4.4 Polyelectrolytes (PEs)

Fig. 11 illustrated the recently developed PE-based EELs in PSCs, where they can be divided into three main types including, PFN- and polythiophene (PT)-based CPEs and non-conjugated PEs. In contrast to neutral polymeric EELs (Section 4.3), most of the PE-based EELs can be simply dissolved in alcohol-based solvents.

For PFN-based CPEs, Huang *et al.* investigated a series of amino *N*-oxide-functionalized PF copolymers (PNOs) comprising fluorene and pyridinyl moieties.[229] They revealed that the amino *N*-oxide groups enable PNOs to have better charge-transporting properties than their amino functionalized parent polymers (PNs). In addition, the different linkages of pyridinyl units in PNOs play an important role on the resulting electronic properties. Consequently, the PCE of PSC using $PF_6NO_{25}Py$ EEL is 1.7 times higher than that without using it. They also utilized PFN-Br to modify a ZnO EEL, optimizing the electrical contact between ZnO and BHJ. As a result, the performance of a PBDT-DTNT:$PC_{71}BM$ device was improved from 6.10% to 8.40% (**Table 2**).[230] Recently, a series of zwitterionic PFN-based CPEs comprising the same sulfobetaine groups on the side-chains and different conjugated moieties have also been reported as efficient EELs in PSCs.[231] The nature of the conjugated backbone and the polar zwitterionic side-chains were found to be important for interfacial

modification. As a result, a PFNSO EEL utilizing a fluorene moiety afforded a PTB7:$PC_{71}BM$ device with PCE as high as 8.74% (**Table 2**).

PT-based CPEs have also been investigated. Buriak *et al.* adopted an aforementioned eLbL approach to prepare P3(TBP)HT$^+$:PEDOT:PSS$^-$ (similar to PTCDI$^+$:PEDOT:PSS$^-$ introduced in Section 4.1) composite films from P3(TBP)HT$^+$Br$^-$ and PEDOT:PSS.[232] Such EEL remarkably improved device stability, in which 97% of the original PCE could be maintained over 1000 h of storage in air. Soon after, Yang *et al.* also delineated a similar CPE-surfactant complex fabricated from PTMAHT and sodium dodecyl-benzenesulfonate (SDS).[233] Recently, Maes *et al.* delineated imidazolium-substituted PT-based EELs,[234] in which the polymer chain lengths of such CPEs have a substantial influence on the resulting device performance. P3(IMD)HT-Br with a relatively high molecular weight showed the best PCE, outperforming other CPEs. Meanwhile, Emrick *et al.* also developed a series of zwitterionic PT-based EELs, PTBTSB-1 and PTBTSB-2.[235] With the analysis from the near edge X-ray absorption fine structure (NEXAFS) spectra, they unveiled that the interfacial dipoles formed by these CPEs contributed to the electrostatic self-alignment of zwitterionic side-chains near the metal surface, where the negative charge of the zwitterion points to the surface.

Very recently, Emrick *et al.* have further introduced non-conjugated azulene-triazole (A-T) PATSB EELs.[236] The density of A-T along the polymer chains greatly influences its optical properties and excitonic behavior, which results in increased device performance based on the A-T density in the PATSB EELs. As a matter of fact, the PATSB-3 with the highest A-T content (~75 mole%) enables the derived PTB7:$PC_{71}BM$ device to have a high PCE of 7.9%.

4.5 Organic-Inorganic hybrids

In the past few years, there has also been some significant progress made in organic-inorganic hybrid thin-film EELs for PSCs. Chen *et al.* have reported the synthesis of a hybrid Zn-C_{60} EEL by reacting the fullerene precursor (PCBE-OH) with zinc acetate (Zn(Ac)$_2$) (**Fig. 12a, left**).[237] From the XPS measurements, C_{60} is shown to be concentrated at the Zn-C_{60} surface, enabling the upper organic BHJs to have better compatibility at this corresponding interface. This C_{60}-doped species also possessed a deeper-lying LUMO level (4.53 eV) than that of pristine ZnO (4.14 eV), which serves as new transport pathways for electrons (**Fig. 12a, right**). As a result, the P3HT:$IC_{60}BA$ BHJ device with Zn-C_{60} EEL showed much improved performance (5.26% to 6.60%). This effect is also applicable to
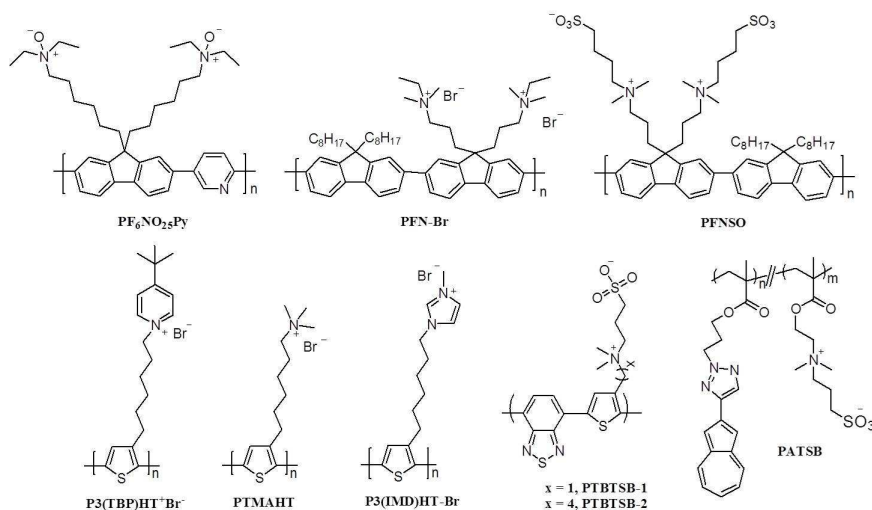

Fig. 11 Recently developed polyelectrolyte-based EELs for PSCs.

PTB7:PC$_{71}$BM (6.65% to 8.21%), and PTB7-Th:PC$_{71}$BM based devices (7.64% to 9.35%) compared to the pristine ZnO EEL device (**Table 2**).

Xie *et al.* have also introduced a hybrid ZnO-PFEP EEL by sensitizing ZnO nanocrystals (NCs) with a blue fluorescent conjugated PFEP, where PFEP not only prevents the aggregation of ZnO NCs through its attached phosphonate groups but also enhances the conductivity of ZnO NCs *via* charge transfer doping driven by electron-chemical potential equilibrium (**Fig. 12b**).[238] Due to the light excitation of PFEP sensitizer, the charge transfer doping even became more pronounced under illumination and enabled 44-70% enhancement in performance compared to the ZnO devices. In addition, the conductive ZnO-PFEP allowed a thick EEL to be used in large-scale printable PSCs, which led to a high-efficiency (6.26%) doctor-blade printed PCDTBT:PC$_{71}$BM device. This value is comparable to those of spin-cast devices.

Similarly, Fang *et al.* developed an organic-inorganic hybrid EEL, CdS·BCP, which combines the high electron mobility of CdS and decent hole blocking property of BCP (**Fig. 12c**).[239] Note that the derived inverted PTB7:PC$_{71}$BM device showed much improved stability compared to that of the conventional PEDOT:PSS device. Only 14.2% decay of PCE was observed after 3264 h storage in a glovebox, while the one based on PEDOT:PSS showed 45.4% degradation.
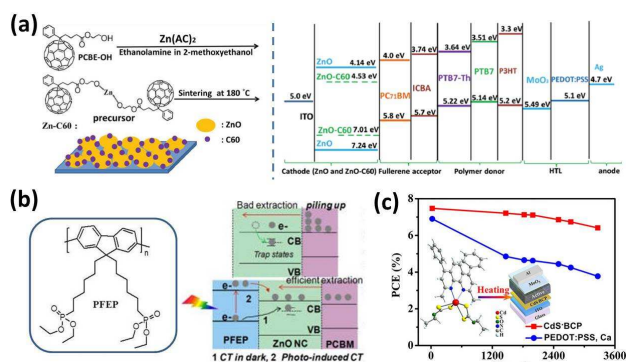
Fig. 12 (a) Reaction scheme of Zn-C$_{60}$ and the energy level diagram of the derived device. Adapted with permission from ref. 237 Copyright 2013 Wiley-VCH Verlag GmbH & Co. KGaA. (b) Structure of PFEP EEL and the illustration of its induced charge-transfer mechanism driven by electron-chemical potential equilibrium. Adapted with permission from ref. 238 Copyright 2014 American Chemical Society. (c) The precursor structure for CdS·BCP EEL and its derived device configuration and stability measurement. Reprinted with permission from ref. 239 Copyright 2013 American Chemical Society.

4.6 GOs

Due to tailorable energy levels and electronic properties, solution-processed GO-based EELs also have shown important advances in the past few years. Dai *et al.* first reported a Cesium-neutralized (GO-Cs) EEL, where the periphery –CO$_2$H groups in GO were neutralized by Cs$_2$CO$_3$ and replaced with –CO$_2$Cs groups (**Fig 13a**).[156] GO-Cs has a much lower WF of 4.0 eV than the pristine GO (4.7 eV), enabling it as an efficient

EEL for extracting electrons from PCBM (4.1 eV) in BHJs. A conventional P3HT:PC$_{61}$BM device with GO HEL and GO-Cs EEL showed a high PCE of 3.67%, outperforming that of the device using PEDOT:PSS HEL and LiF EEL (**Fig 13a**).

Later, Yang and co-workers have described the first GO-fullerene composite EEL, rGO-pyrene-PC$_{61}$BM, where the pyrene-PC$_{61}$BM was linked to r-GO through pyrene as an anchor *via* π−π interaction (**Fig. 13b**).[240] Such non-covalently functionalized r-GO has a low WF (4.4) eV and decent solution processability due to improved dispersion of r-GO in DMF. The P3HT:PC$_{61}$BM device using this EEL showed increased PCE (15% enhancement) compared to those of the devices using r-GO or pyrene-PCBM as EELs.

Meanwhile, Silva *et al.* reported rGO-TMO hybrid EELs, TiO$_2$-rGO and ZnO-rGO (**Fig. 13c**).[241, 242] Such composites could afford smooth film formation since the graphene layers
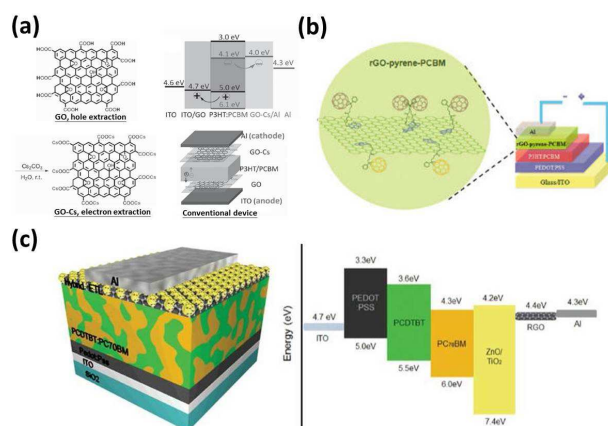
Fig. 13 (a) Synthetic route of GO-Cs and its derived device structure and energy diagram. Adapted with permission from ref. 156 Copyright 2012 Wiley-VCH Verlag GmbH & Co. KGaA. (b) Illustration of possible conformations of rGO-pyrene-PCBM and its derived device structure. Reprinted with permission from ref. 240 Copyright 2013 American Chemical Society. (c) Device structure and energy level diagram of the device using TiO2-rGO/ZnO-rGO EEL. Adapted with permission from ref. 242 Copyright 2014 Wiley-VCH Verlag GmbH & Co. KGaA.

wrap around the TMO NPs. In addition, the loaded r-GO could contribute to extra CT pathways through the TMO NPs. Due to their appropriate energy levels and enhanced electrical conductivities, the PTB7:PC$_{71}$BM and PCDTBT:PC$_{71}$MB devices derived from such EELs showed higher PCEs than those based on TMO alone. Impressively, a high PCE (~3%) large area module cell (3920 mm^2) was demonstrated by using ZnO-rGO EEL, exhibiting a 20% enhancement compared to those of the pristine TMO devices.

4.7 Solution-processed TMOs

In contrast to the diverse development of TMO HELs, the recent progress in TMO EELs is centred around TiO$_2$ and ZnO due to their decent ambient stability, optical transparency, and suitable WFs that match the PCBMs in BHJ.[174] To be suitable for low-temperature

Table 2. Device Characteristics of representative PSCs using versatile EELs introduced in this review.

Device Structure	V_{OC}	J_{SC}	FF	PCE	Ref.
	(V)	(mA/cm^2)		(%)	
ITO/PEDO:PSS/PTB7-Th:PC$_{71}$BM/PDINO/Al	0.8	15.45	0.68	8.35	200
ITO/PEDO:PSS/PCDTBT:PC$_{71}$BM/3TPA-FEP/Al	0.92	11.98	0.65	7.21	203
ITO/FTBTF-N/PTB7:PC$_{71}$BM/MoO$_3$/Al	0.74	17.23	0.72	9.22	137
ITO/PEDOT:PSS/PBDTTT-C-T:PC$_{71}$BM/PEGN-C$_{60}$/Al	0.79	14.79	0.63	7.45	205
ITO/PEDOT:PSS/PBDTTT-C-T:PC$_{71}$BM/DMAPA-C$_{60}$/Al	0.79	14.89	0.63	7.42	206
ITO/PEDOT:PSS/PBDTTT-C-T:PC$_{71}$BM/PCBDANI/Al	0.78	17.29	0.57	7.69	207
ITO/PEDOT:PSS/PIDTT-DFBT:PC$_{71}$BM/Bis-C$_{60}$/Ag	0.96	12.7	0.62	7.66	123
ITO/PEDOT:PSS/PTB-7:PC$_{71}$BM/CPTA/Al	0.74	16.95	0.63	7.92	214
ITO/PEDOT:PSS/PTB7-Th:PC$_{71}$BM/C$_{60}$-SB/Ag	0.75	16.89	0.68	8.57	215
ITO/PEDOT:PSS/PTB7-Th:PC$_{71}$BM/C$_{60}$-N/Ag	0.78	16.83	0.71	9.35	215
ITO/FPI-PEIE/PTB7-Th:PC$_{71}$BM/MoO$_3$/Ag	0.8	16.15	0.72	9.62	216
ITO/ZnO/PEI/PTB7:PC$_{71}$BM/MoO$_3$/Ag	0.73	17.19	0.7	8.76	217
ITO/PFN/PTB7:PC$_{71}$BM/MoO$_3$/Al	0.75	17.46	0.7	9.21	218
ITO/PEDOT:PSS/P3HT:IC$_{60}$BM/PFCn6:K$^+$/Ca/Al	0.89	11.65	0.73	7.50	219
ITO/PFEN-Hg/PTB7:PC$_{71}$BM/MoO$_3$/Al	0.74	17.37	0.71	9.11	220
ITO/PFN-OX/PBDTTT-C-T:PC$_{71}$BM/MoO$_3$/Au	0.77	17.7	0.67	9.13	221
ITO/ZnO/PFN-OX/PTB7:PC$_{71}$BM/MoO$_3$/Al	0.75	16.63	0.74	9.28	222
ITO/ZnO/PFN-Br/PBDT-DTNT:PC$_{71}$BM/MoO$_3$/Ag	0.75	17.40	0.61	8.40	230
ITO/PEDOT:PSS/PTB7:PC$_{71}$BM/PFNSO/Al	0.73	16.38	0.73	8.74	231
ITO/ZnO-C$_{60}$/PTB7:PC$_{71}$BM/MoO$_3$/Ag	0.73	15.41	0.73	8.21	237
ITO/ZnO-C$_{60}$/PTB7-Th:PC$_{71}$BM/MoO$_3$/Ag	0.80	15.73	0.74	9.35	237
ITO/ZnO-PVP/pDTG-TPD:PC$_{71}$BM/MoO$_3$/Ag	0.86	14.00	0.67	8.10	244
ITO/ZnMgO/PTB7:PC$_{71}$BM/MoO$_3$/Ag	0.74	16.78	0.67	8.31	247
ITO/ZnO NPs/pDTG-TPD:PC$_{71}$BM/MoO$_3$/Ag	0.86	14.10	0.67	8.10	248

processing, a sol-gel method is generally employed for preparing TMO EELs.

As mentioned in Section 2.3, such a sol-gel TiO$_2$ had been applied to inverted PSCs and demonstrated to function as an optical spacer to enhance the light-harvesting of BHJ.[94] In addition to the sol-gel route, a low-temperature (130-170 °C) atomic layer deposition (ALD) technique with better printing production potential was recently employed by Zhu et al. to fabricate TiO$_2$ EEL.[243] Similar to those reported for organic-inorganic hybrids (Section 4.5), So and Reynolds et al. lately have reported a surface-modified sol–gel ZnO EEL, ZnO-PVP, and demonstrated a device with high PCE of over 8% from the derived pDTG-TPD:PC$_{71}$BM device (**Table 2**).[244] However, the PVP, having a small surface energy, will emerge to the thin-film surface during the ZnO-PVP film formation, which creates an undesired interfacial Φ_B for charge extraction. It is necessary to use UVO treatment to remove surface PVP.

Recently, atomically doped ZnO EELs have also attracted certain attention. Sirringhaus et al. have introduced a series of Sr/Ba-doped ZnO EELs prepared from the sol-gel route with metal alkoxide molecular precursors.[245] Such doped ZnO EELs can circumvent the required light-soaking procedure for pristine ZnO because the Sr/Ba doping can effectively supress the oxygen absorption at the oxygen vacancy sites on ZnO surface to reduce electron trapping associated with oxygen adsorption. Later, Olson et al. described a sol-gel MgZnO EEL that demonstrated the importance of Mg content on the resulting WF and E$_g$.[246] Meanwhile, Zheng et al. also showed that Mg doping can tailor the WF and E$_g$ of a resultant Zn$_{1-X}$Mg$_X$O EEL (**Fig. 14**).[247] By carefully adjusting the Mg doping content, a high-performance (8.31%, **Table 2**) PTB7:PC$_{71}$BM device with

much improved ambient stability compared to PEDOT:PSS device was achieved.

Colloidal ZnO NPs with a nano-crystalline phase have also been widely employed to prepare ZnO EELs. ZnO NPs were synthesized by reacting Zn(Ac)$_2$ dihydrate precursor solution with a strong base and tetramethyl-ammonium hydroxide. However, the ZnO thin-film prepared from this method contained significant amount of defects, as a result, sequential UVO treatments were required. So and Reynolds et al. have recently used such UVO-treated ZnO NP EELs to realize a high-efficiency DTG-TPD:PC$_{71}$BM device (8.10%, **Table 2**).[248] Similarly, Yang et al. have also employed such UVO-treated ZnO NP EELs to demonstrate a stable PTB7:PC$_{71}$BM device with a PCE of 7.34%.[249]

Beside TiO$_2$ and ZnO, Riedl et al. have used tetrakis(diethylamino)tin (TDEASn) as a precursor with a small amount of acetylacetone as stabilizer to make a sol-gel SnO$_X$ EEL.[250] This SnO$_X$ EEL exhibited a low WF (4.1 eV) and room temperature solution processability. Devices using SnO$_X$ EELs
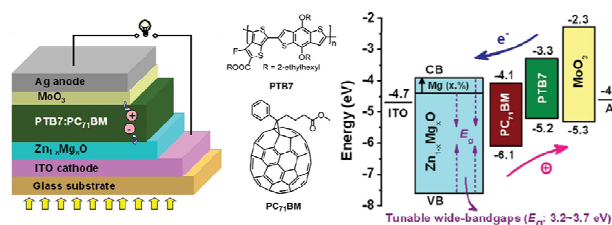

Fig. 14 (Left) Zn$_{1-X}$Mg$_X$O EEL-based device structure, (Middle) structures of PTB7 and PC$_{71}$BM, and (Right) the corresponding energy levels. Adapted with permission from ref. 247 Copyright 2014 Wiley-VCH Verlag GmbH & Co. KGaA.

can deliver a comparable performance to that of TiO_X devices but with much-enhanced thermal stability in air. Very recently, Choy *et al.* have revealed that MoO_3 and V_2O_5 HELs can be converted to EELs by intercalating with Cesium (Cs).[197] The more Cs intercalated in TMOs, the lower the resultant WF. Consequently, over 1.1 eV WF shifting of Cs_XMoO_3 (from 5.35 eV to 4.24 eV) and $Cs_XV_2O_5$ (from 5.43 eV to 4.15 eV) could be achieved in PBDTDTTT-S-T:PC$_{71}$BM devices made with Cs_XMoO_3 (7.32%) and $Cs_XV_2O_5$ (7.49%) EELs.[197]

5. Self-assembled Monolayers (SAMs)

Interfacial modifications with functional SAMs between the organic absorbers and electrodes/charge-transporting interlayers are very important in enhancing charge extraction and overall performance. Different kinds of SAMs (p- or n-type) can be used according to the type of promoted charges. Recently, increasing attention has been paid to developing organic semiconductors with deep-lying HOMO levels in order to enlarge the V_{OC} of devices. However, the same effect can also be achieved by directly modifying the anode interfacial contact with proper p-type SAMs.[251] The recent development in p-type SAMs is mainly focused on modifying the surface of ITO anodes. For instance, a series of dipolar phosphonic acid SAMs[252] and silane-tethered bis(fluoroaryl)-amines[253] have been introduced to modify the ITO WF and its surface, in which the ITO WF (4.6-4.7 eV) can be effectively increased to 5.2-5.3 eV by those p-type SAMs to provide a better energy level alignment with the used polymers in BHJ layers. Also, they can simultaneously modulate the carrier lifetime in BHJ and the V_{OC} of devices. Besides oligomers, polymeric surface modifiers have also been investigated. You *et al.* introduced poly(3-methylthiophene) (P3MT) SAMs that are covalently

bonded to the ITO surface *via* surface-initiated Kumada catalyst-transfer polycondensation (SI-KCTP). This is beneficial to prevent delamination during the processing of sequential layers, and the material also serves as a sufficient HEL for PSCs (**Fig. 15a**).[254]

N-type SAMs can be applied to certain EELs that are known to contain defects with varied stoichiometries and surface terminations. The application of n-type SAMs can passivate the TMO EEL surface. For example, Jen *et al.* have utilized a fullerene-SAM (C$_{60}$-SAM) to modify ZnO surface *via* simple spin-coating to enhance the electronic coupling of this interface, leading to a much-improved device performance.[76, 255] Lately, carboxylated fullerene SAMs have also been used by Kim *et al.* to modify TiO_X to deliver a smoother and more hydrophobic surface with reduced trap-states compared to pristine TiO_X (**Fig. 15b**).[256]

In addition to fullerene-based SAMs, Olson *et al.* have recently introduced dipolar benzyl phosphonic acids to passivate the ZnO surface to reduce oxygen adsorption, which can also slightly tune the WF of ZnO (0.2 eV) to result in a smaller energy barrier for electron injection to enhance device performance.[257] Cho *et al.* also showed that SAMs could be used to tailor the surface energy of ZnO to modulate the BHJ morphology evolution.[72] Alternatively, Chen *et al.* have introduced a tetrafluoroterephthalic acid (TFTPA) SAM to modify the ZnO surface for increasing adhesion of the fullerenes atop the BHJ. This also created a fullerene-rich surface on the modified ZnO to improve charge extraction and device performance. (**Fig. 15c**).[258]

6. Interconnecting Layers (ICLs) in Polymer Tandem Cells (PTCs)

As discussed in Section 2.3, the major obstacle for achieving high-performance PSC is the thin-film structure that limits light-harvesting efficiency. In this regard, PTCs can be used to overcome this difficulty by stacking multi-junctions in parallel or in series connection to broaden the light absorption spectrum and enhance light-harvesting efficiency of devices, improving performance.[259, 260] One of the critical components for tandem devices is the interconnection layer (ICL) that connects the subcells. In principle, the ICL not only functions for collecting electrons from one subcell and holes from another, but also as a charge recombination site to avoid potential loss of tandem devices.[261] For an ideal PTC, the ICL and subcells should form an Ohmic contact, and be able to handle multilayer integration by solution processing. To develop solution processable ICLs having superior solvent resistance is one of the prerequisites to prevent the erosion of bottom subcells during the fabrication of top subcells. Several detailed reviews of tandem developments can be found in recent articles.[259, 260]
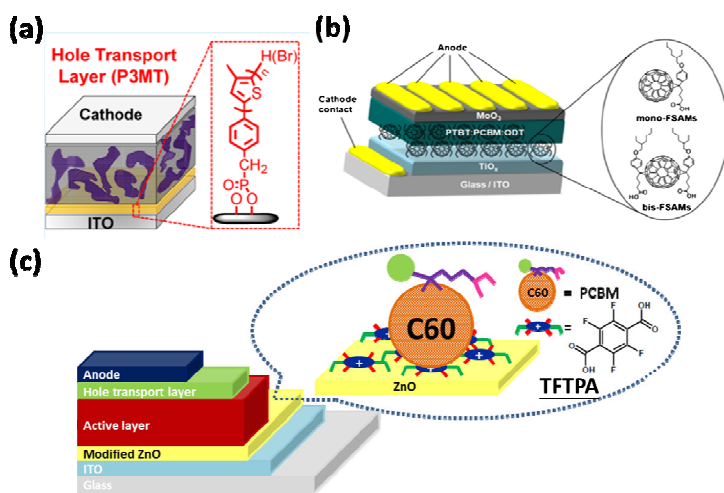

Fig. 15 (a) Structure of P3MT and its derived device configuration. Adapted with permission from ref. 254 Copyright 2012 American Chemical Society. (b) Structure of carboxylated fullerene SAMs and their derived device structures. Reprinted with permission from ref. 256 Copyright 2013 Elsevier. (c) Illustration of the interactions between TFTPA and PCBM, and the derived device architecture. Reprinted with permission from ref. 258 Copyright 2013 American Chemical Society.
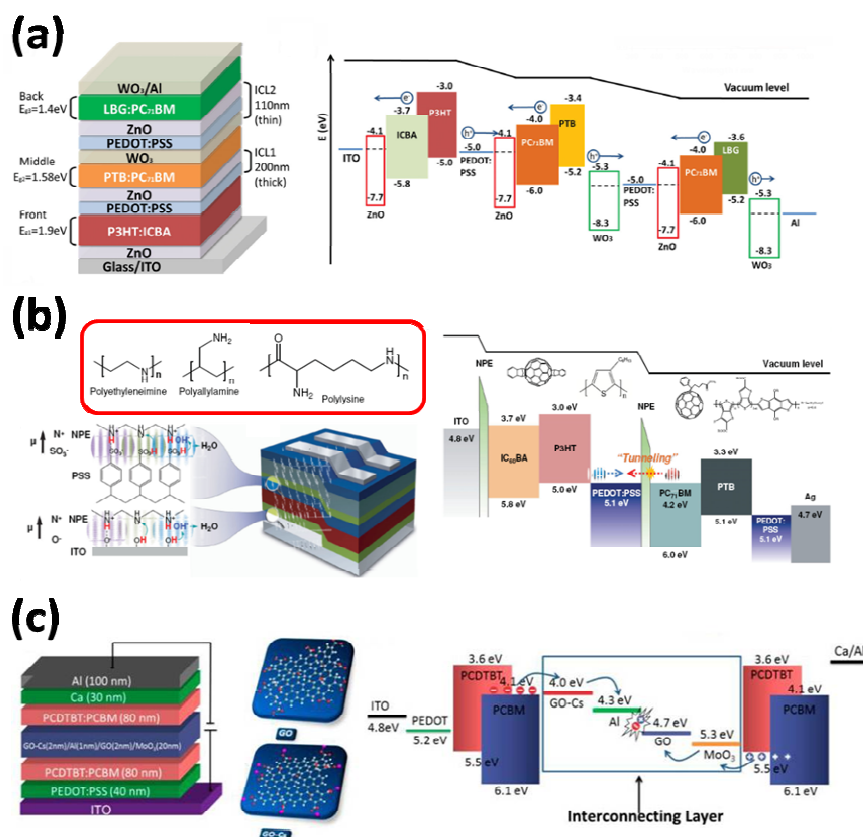
Fig. 16 (a) Device structure of the state-of-the-art triple-junction PTCs and the corresponding energy level diagram. Adapted with permission from ref. 264 Copyright 2014 Wiley-VCH Verlag GmbH & Co. KGaA. (b) Structures of employed non-conjugated PEs, polymers and fullerenes for BHJ layers, double-junction PTC, and the relevant energy level diagram. Adapted with permission from ref. 269 Copyright 2013 Wiley-VCH Verlag GmbH & Co. KGaA. (c) Device structure and energy levels of the PTCs employing GO-based ICL. Adapted with permission from ref. 270 Copyright 2014 American Chemical Society.

In this section, we will only highlight the latest progress of solution-processable ICLs for PTCs.

At present, combined TMOs (ZnO or TiO_X) and PEDOT:PSS are still the most frequently used materials as solution processable ICLs for PTCs due to their robustness and orthogonal solvent processability. Yang *et al.* reported in 2013 a record high PTC with a certificated PCE value of 10.6% based on such a ZnO/PEDOT:PSS ICL.[262] Meanwhile, Janssen and co-workers have utilized similar ICL to demonstrate a highly efficient (9.6%) triple-junction PTC, where the middle and back sub-cells comprised the same BHJ layers.[263] Very recently, Yang *et al.* have described a state-of-the-art triple-junction PTC with a PCE of over 11% by combining three BHJs with complementary absorption (**Fig. 16a**).[264] In such a device, the wide E_g BHJ, P3HT:$IC_{60}BA$ (E_{g1} = 1.9 eV) was placed in the front subcell, followed by middle subcell of PBDTT-TT:$PC_{71}BM$ (E_{g2} = 1.58 eV) with ZnO/PEDOT:PSS as an ICL while PDTP-DFBT:$PC_{71}BM$ (E_{g3} = 1.4 eV) BHJ was used as the back subcell with a WO_3/PEDOT:PSS/ZnO ICL to overcome mismatched energy levels between low E_g polymers (i.e., PBDTT-TT and PDTP-DFBT) and PEDOT:PSS. This

design of cascade E_g (i.e., E_{g1} > E_{g2} > E_{g3}) facilitates the harvesting of photon energy, resulting in a higher theoretical efficiency limit relative to those of single- and double-junction cells.

In addition to TMOs, recent developments in organic surfactants have also shown the merits of simple processability, chemical diversity, and mechanic robustness for fabricating efficient tandem devices. Kippelen *et al.* recently have demonstrated an ICL consisting of PEIE/PEDOT:PSS, in which the PEIE can modify the interface between it and PEDOT:PSS to provide a large WF contrast (1.3 eV).[265] This ICL also showed low optical absorption and high electrical conductivity to maximize V_{OC} to be the sum of individual cells.[266, 267] The PEIE was also used to modify the surface of MoO_X/Al_2O_3:ZnO nano-laminate bilayer to enable it to function as an efficient ICL.[268] Lately, other non-conjugated PEs (NPEs, **Fig. 16b**) has also been introduced to modify PEDOT:PSS to achieve depletion-free recombination layers in inverted PTCs.[269]

Recently, GO-based ICLs have also been investigated. Huang *et al.* have shown GO can be blended into PEDOT:PSS layer to improve its stickiness for tandem solar cells.[141] More recently, Dai *et al.* have used GO-Cs EEL (discussed in Section 4.6) to form GO-Cs/Al/GO/MoO3 ICL for achieving significantly increased V_{OC} of the derived PTC (**Fig. 16c**) to reach almost 100% of the sum of the subcells' V_{OC}.[270] All these results show the importance of using an efficient ICL to create negligible electrical and/or optical losses and to maximize the V_{OC} values.

7. Interfacial Engineering in Organometal Perovskite Solar Cells (PVSCs)

Recently, the rapid progress in organometal PVSCs has attracted worldwide attention, propelling this organic-inorganic hybrid system to the forefront of next-generation printable photovoltaics.[271-273] The representative organometal perovskite has a crystal structure based on the formula of ABX_3, where A is an organic cation, B is a metal cation, and X is a halide anion, respectively. Accordingly, the optoelectronic properties of a perovskite can be tailored by changing its composition. So far, the organic cations that have been used for forming perovskites

are mainly based on methylammonium (MA) and formamidinium (FA) due to the low steric tolerance space (1.6-2.5 angstroms) for organic cations in three-dimensional perovskites.[274-276] Note that the increased size of FA relative to MA causes certain torsion of perovskite's lattices to result in decreased E_g of the FA-based perovskites.

For the metal cation, divalent Pb is the most commonly used element so far; however, due to its toxicity, it is very critical to find other environmentally friendly metals to replace Pb in perovskites. At present, the divalent Sn is the most promising candidate for replacing Pb^{2+}. Several groups have successfully employed Sn- or partially Sn-based perovskites to acquire reasonable photovoltaic performance (5-10% PCE).[277-281] Nevertheless, the easy oxidation of Sn^{2+} to Sn^{4+} in Sn-based PVSCs results in severe energy loss and unstable device performance. Therefore, significant challenges remain in developing lead-free PVSCs in the future.

With respect to the variation of anions, halide substitution (I, Br, or Cl) has been widely investigated and revealed as an effective way to broaden the E_g of derived perovskites.[274, 282-285] Numerous studies have shown that larger E_g perovskites can be achieved by partially replacing the iodide (I^-) with bromide (Br^-) in the perovskite lattice to result in decent PCEs (over 10%) of the derived PVSCs. On the contrary, the incorporation of chloride (Cl^-) with I^- only resulted in modulated morphology of perovskite thin films without significantly changing its E_g because only negligible Cl^- content was found after annealing due to the decomposition of MACl during thermal conversion.[286-288] It is important to mention that the improved morphology of the perovskite thin film significantly enhances its opto-physical properties, such as the charge carrier lifetime and diffusion length.[289]

Among all perovskites, MA lead triiodide ($CH_3NH_3PbI_3$) is the most frequently studied due to its almost ideal semiconducting properties. It has the combined superior photo-physical properties of inorganic materials and good solution processability of organic materials. It possesses intense light absorption (absorption coefficient over 10^4 cm^{-1}), small exciton binding energy (20-50 meV at room temperature), and long charge carrier diffusion length and lifetime (>1000 nm and >100 ns).[289, 290]

In general, the E_g of $CH_3NH_3PbI_3$ is around 1.5-1.6 eV with a conduction band energy level of -3.9 eV and a valence band energy level of -5.4 eV, which are very similar to the energy levels of most BHJs studied in PSCs. PVSCs were initially investigated in dye-sensitized photovoltaic cells, then gradually evolved into planar thin-film cells with similar device architectures to those used for PSCs, in which the perovskite layer is sandwiched between two charge-transporting interlayers.[291] Therefore, the knowledge accumulated for interfacial engineering in PSCs can be effectively translated into PVSCs. In the following sections, we also summarize the relevant progress of interfacial engineering approaches used in improving the performance of PVSCs.

7.1 Charge-transporting interlayers

As mentioned, a typical PVSC possesses the similar sandwiched configuration to PSCs, while the energy levels of a perovskite are analogous to the energy levels of most studied BHJ systems. However, different to the p-n BHJ in OPVs, a PVSC is typically composed of a p-i-n heterojunction configuration. Similarly, two types of PVSCs can be defined according to the sequence of the employed p/i/n junctions: conventional structure (substrate/HEL
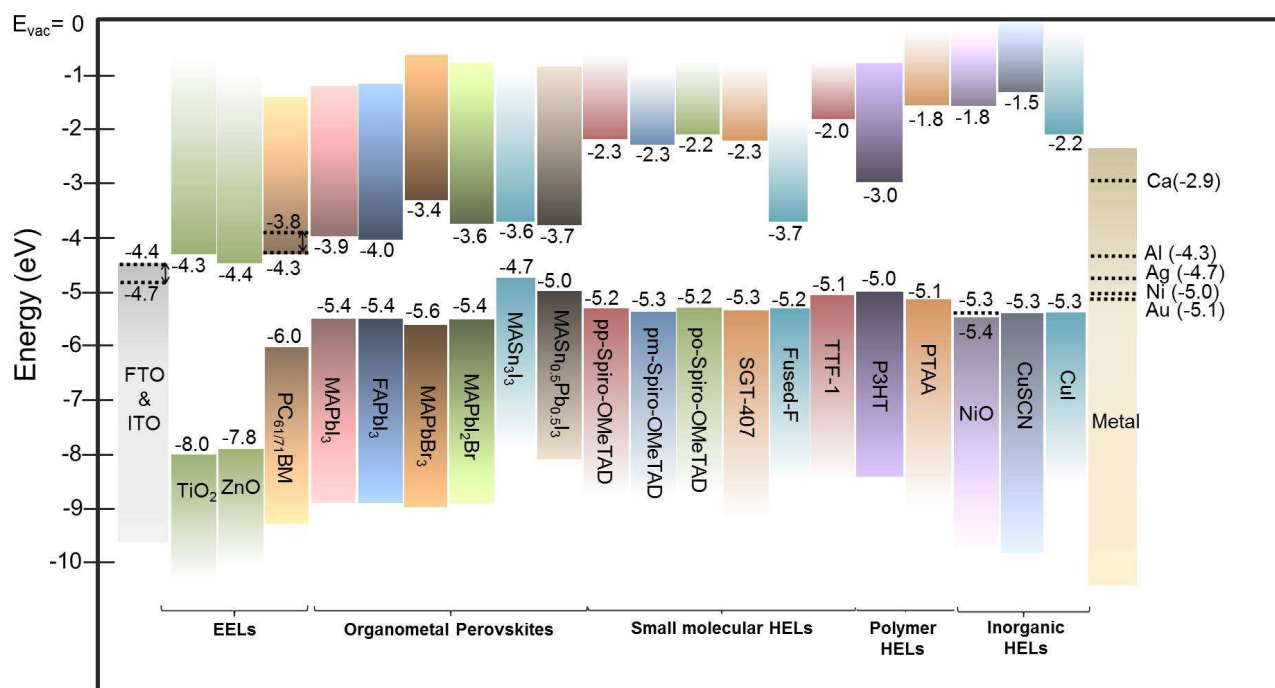

Fig. 17. A summarized energy level diagram of representative organometal perovskites and charge-extraction interlayers. The dotted lines represent the WF of the materials.

(p)/perovskite (i)/EEL (n)) and inverted structure (substrate/EEL (n)/perovskite (i)/HEL (p)). In the following section, we will introduce the recent development of solution-processed interfacial materials in different types of PVSCs. The energy levels of perovskites and the representative HELs and EELs are summarized in **Fig. 17**.

7.1.1 Inverted PVSCs

Inherited from the original mesoporous prototype, TiO$_2$ is the most widely used EEL in inverted PVSCs, whether for a meso-superstructured scaffold or a thin-film structure.[267-268, 292] However, the high temperature (500 °C) sintering process involved for preparing primary mesoporous TiO$_2$ with high crystallinity significantly hinders this structure from being used for flexible polymer substrates. As a consequece, low-temperature processed TiO$_2$ EELs from different chemical routes have been developed to alleviate this problem for inverted PVSCs. Recently, Gratzel and Snaith *et al.* have successfully realized low-temperature, solution-derived TiO$_2$ EELs by utilizing nanocrystalline rutile TiO$_2$ (70 °C) and small NPs of anatase TiO$_2$ (<150 °C), respectively, to afford promising PCEs of 13.7% and 15.9%.[293, 294]

Similar to the applications discussed in Section 5, n-type

SAMs were also employed to passivate the TMO EEL surface to promote better charge extraction and device performance in PVSCs. For example, Snaith and Jen *et al.* have utilized a C$_{60}$-SAM to modify the surface of TiO$_2$ EELs in both meso-superstructured scaffolds and in a thin-film structure to modulate the electron coupling at the TiO$_2$/perovskite interface, reducing the energy loss across this interface (**Fig. 18a**).[295, 296] As a result, the PCE of the meso-superstructured PVSC can be improved from 10.2% to 11.7% while the PCE of the thin-film PVSC can be enhanced from 12.7% to 17.3% with greatly reduced hysteresis. It is important to note that the anomalous hysteresis has recently been raised as an important issue for PVSCs, especially for the TiO EEL-based inverted PVSCs.[297] It is considered to originate from the traps states existing at the perovskite/charge-transporting layer interfaces, defects within perovskites, and the ferroelectric properties of perovskites. In addition to the SAM-modifications, various methods have also been exploited to decorate TiO-based EELs to reduce the hysteresis of fabricated device.[298-299] On the other hand, Yang *et al.* have reported that the insertion of graphene quantum dots (GODs) into the TiO$_2$/perovskite interface can result in a much faster electron extraction between perovskite and TiO$_2$ because
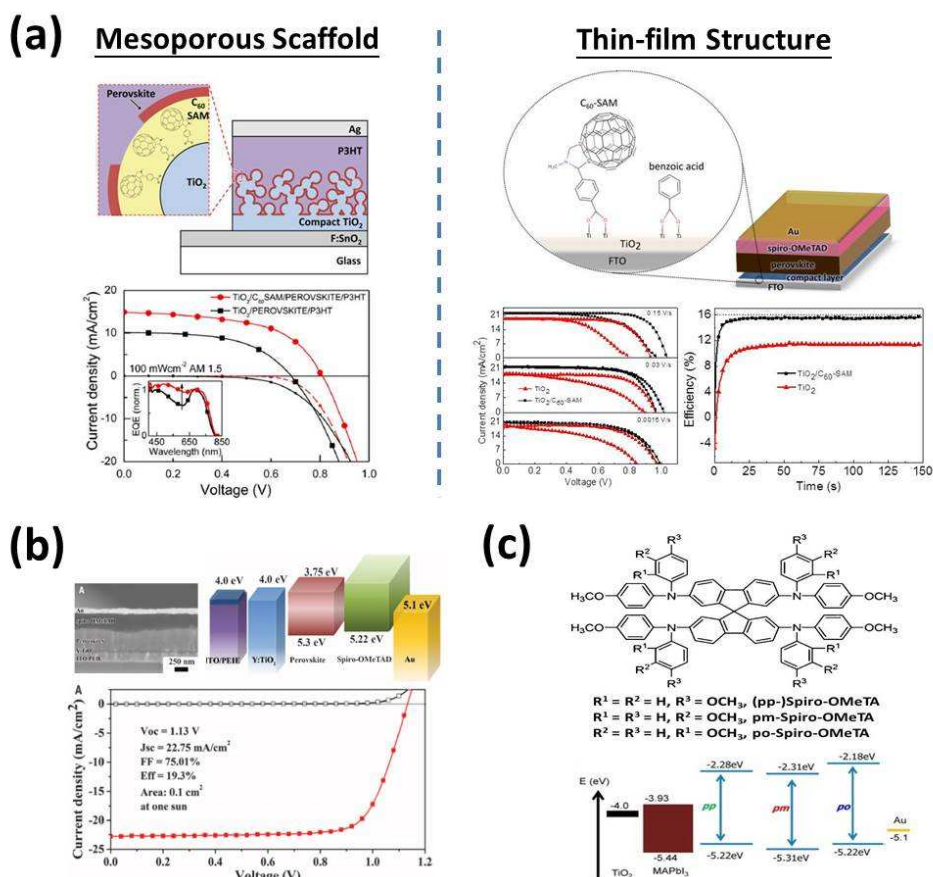
Fig. 18 (a) Structure of the C60-SAM modified PVSCs and the corresponding *J-V* characteristics. Adapted with permission from ref. 295 & 296 Copyright 2014 American Chemical Society. (b) SEM cross-sectional image, energy level diagrams, and *J-V* characteristics of the PVSC with PCE over 19%. Adapted with permission from ref. 302 Copyright 2014 AAAS. (c) Structures of spiro-OMeTAD derivatives and their corresponding energy level diagrams. Adapted with permission from ref. 306 Copyright 2014 American Chemical Society.

the GODs interlayer functions as a glue to facilitate the electronic coupling between them.[300] Consequently, the PCE of GODs-inserted PVSC can be improved from 8.81% to 10.15%.

The atomically-doped TMO EELs introduced in Section 4.7 have also been used to achieve great success in PVSCs.[301, 302] The efficacy of doping EELs have recently been unveiled by Yang *et al.*[302] They employed an yttrium-doped TiO_2 (Y-TiO_2) EEL to improve charge extraction to achieve a very high PCE of ~19.3% (**Fig. 18b**). Note that in their reported device configuration, a thin PEIE was inserted between ITO and EEL to tune the ITO WF for facilitating charge extraction.

Besides TiO_2, Kelly *et al.* recently have successfully utilized a room-temperature-processed ZnO EEL, prepared from a ZnO NP precursor, to afford a high PCE of 15.7% in an inverted PVSC.[303] It enables the device to be processed at low temperature throughout fabrication, which is beneficial for the fabrication of flexible PVSCs. As a result, a high-performance flexible PVSC with a PCE of 10.2% has been achieved. From all these results, the development of low-temperature processable EELs was proven to be very critical for fabricating printable inverted PVSCs.[304]

Due to the advantages of low-temperature and orthogonal solvent processability and appropriate energy levels, organic HELs are prevalently used in the inverted PVSCs. However, due to their intrinsically low mobility, proper doping of organic HELs is usually required to achieve higher conductivity for enhancing device performance. Among the p-type organic semiconductors, the small molecular spiro-OMeTAD is the most commonly used.[272, 273, 291] It has been well documented that doping spiro-OMeTAD with oxygen can effectively increase its conductivity and enable higher device performance. However, LiTFSI must be used as a counterion in this process to facilitate the oxidative reaction between spiro-OMeTAD and O_2. This complicates the doping process and makes it difficult to be reproduced. To alleviate this problem, McGehee *et al.* have recently described a dicationic spiro(TFSI)$_2$ to simplify the doping process.[305] By forming pre-oxidized spiro-OMeTAD, spiro(TFSI)$_2$ can replace LiTFSi to provide an easier way for controllably increasing the conductivity of HEL without exposure to O_2.

On the other hand, proper molecular design of organic HELs will also have a critical influence on the charge extraction efficiency. As an example, Seok *et al.* have lately elucidated the importance of HEL molecular structures on device performance by systematically changing the side-chain (-OMe) position in the spiro-type arylamine HELs (**Fig. 18c**).[306] The -OMe groups linked at the ortho position enabled the device with the best PCE of 16.7%. This was attributed to its best efficiency in electron-blocking as a result of its high-lying LUMO. In addition to the spiro-type HELs, other types of small molecules such as carbazole-based derivatives (such as SGT-407)[307-308], quinolizino acridine-based molecules (Fused-F),[309] and tetrathiafulvalene derivatives (TTF-1)[310] were also introduced as efficient HELs in PVSCs to produce decent PCEs (**Fig. 17**). It is worth to note that the tetrathiafulvalene derivative (TTF-1) can serve as a dopant-free HEL to significantly enhace device stability in ambient conditions at a relatively high humidity of ~40%.[310]

Polymer-based EELs have also been employed in PVSCs. However, at present, the PCEs of the PVSCs based on them are generally lower than the devices derived from the small molecular spiro-OMeTAD, which might be due to the inferior molecular packing and mobility of polymers relative to small molecules. The previous result from Seok *et al.* has elucidated the importance of intrinsic mobility of polymer-based HELs on affecting charge-collection and performance of devices, in which four different polymers (P3HT, PCDTBT, PCPDTBT, and PTAA) were systematically investigated.[311] Lately, the diketopyrrolopyrrole-based[312] and PF-based[313] HELs were also reported by Park and Yang *et al.* respectively, to afford comparable PCEs to the values of spiro-OMeTAD-based PVSCs.

In addition to organic semiconductors, the inorganic counterpart also attracts considerable research interests due to its high mobility and low cost. Kamat *et al.* first applied solution-processed copper iodide (CuI) as a HEL in inverted PVSC to afford a decent PCE of 6% with enhanced photocurrent stability.[314] Meanwhile, Gratzel *et al.* demonstrated that the low-temperature solution-processed copper thiocyanate (CuSCN) can serve as an efficient HEL in inverted PVSC to yield a promising PCE of 12.4%.[315] It is worth to note that all these inorganic-based HELs are dopant-free, indicating their great potential in the future development.

7.1.2 Conventional PVSCs

Similar to the conventional PSCs, PEDOT:PSS is also the most widely used HEL in conventional PVSCs because of its high transparency, appropriate energy levels, and, more importantly, the compatibility with organic-inorganic hybrid perovskite.[316-320] To further enhance the charge selectivity of PEDOT:PSS HEL, Bolink *et al.* recently employed another thin electron-blocking layer composed of polyarylamine (polyTPD) to construct an efficient bilayer-type HEL.[318] As a result, the derived device exhibited a decent PCE of 12% with a large V_{OC} of 1.05 V. On the other hand, Lee *et al.* reported a modified PEDOT:PSS hybrid with a perfluorinated ionomer (PFI) to serve as an efficient HEL for PVSCs.[321] They revealed that the blended PFI could be self-organized on the film surface to enable better energy level alignment at the HEL/perovskite interface to enhance device performance. Consequently, PCEs of 11.7% and 8.0% can be realized on the ITO and flexible substrates with large V_{OC} of 0.98 V and 1.04 V, respectively, surpassing the value of control PVSC.

Besides organic PEDOT:PSS, inorganic NiO_X was another frequently used HEL for PVSC both in a meso-superstructured scaffold or a thin-film structure.[322-324] For example, Guo *et al.* first realized a conventional PVSC with a mesoporous NiO_X HEL showing a high PCE of 9.51% with a large V_{OC} of 1.04 eV while Yang *et al.* utilized a planar NiO HEL prepared from sol-gel NiO NCs to afford a decent PCE of 9.11% in thin-film PVSS.[323, 324] Very recently, Jen *et al.* demonstrated that the PCE of NiO_X-based PVSC can be further enhanced to 15.4% by using a Cu-doped NiO_X (Cu:NiO_X) HEL as a result of its largely increased conductivity.[325]

The NiO_X HELs developed to date generally involve a high temperature (300-500 °C) annealing process. In this regard, the

development of low-temperature processed NiO_X HELs has become an important research focus as of late. Guo *et al.* recently successfully used a low-temperature sputtered NiO_X HEL to improve the PCE of the aforementioned mesoscopic NiO-based PVSC to 10.7%.[326] Moreover, by carefully doping the sputtered HEL with a <10% oxygen flow ratio, an even higher PCE of 11.6% can be achieved. All these results and the abovementioned $Y\text{-}TiO_2$ EEL manifest the importance of proper doping for achieving more efficient charge-transporting interlayers to improve the performance of PVSCs.

Currently, the EELs used in conventional PVSCs for high performance are mainly composed of fullerene derivatives, such as C_{60}, $PC_{61}BM$, or $PC_{71}BM$, due to their room-temperature and orthogonal solvent processability as well as decent electron mobility.[316-320] A high PCE of 16.3% was recently realized in a conventional perovskite/$PC_{71}BM$ thin-film PVSC by Wu *et al.*, in which the fullerene interlayer was carefully treated *via* a solvent annealing procedure.[327]

Notably, various buffer layers discussed in PSCs have also been introduced at the fullerene/electrode interface to simultaneously improve charge extraction and tune the WF of used electrodes. These cathode-independent interlayers can allow the usage of stable metals such as Ag to be the top electrode for achieving enhanced device efficiency and stability. For example, Jen *et al.* applied Bis-C_{60} surfactant to align the energy levels at the $PC_{61}BM$/electrode interface.[281, 284, 320, 325, 328] Similarly, Brabec *et al.* utilized PEIE and PDINO EELs to enhance the PCEs of derived PVSCs to 12-13%.[329, 330] Very recently, Rhodamine 101 zwitterion and PFN derivative have also been successfully utilized by Ouyang and Yip *et al.* to improve the PCEs to surpass 13% and 15%, respectively.[331, 332] These low-temperature processed PEDOT:PSS HELs and fullerene-based EELs are ideal for use in a conventional configuration for fabricating high-performance flexible PVSCs.[317, 333, 334] PCEs of > 9% have already been demonstrated in such device architecture by Yang and Jen *et al.,* by using optimized perovskite deposition procedures.[317, 334] All these results highlight the importance of using interfacial layers to significantly enhance the performance of PVSCs.

7.2 Perovskite Interfaces

Beyond the employment of proper charge-transporting interlayers, the perovskite interfaces also significantly influence the device performance and stability. As mentioned in Section 7.1.1, modification of perovskite interfaces can greatly improve the device performance and reliability. Due to the crystalline nature of perovskites, significant attention has been paid to passivation of the perovskite surface to ensure optimum charge transport/extraction across the corresponding interfaces..

Snaith *et al.* have shown iodopentafluorobenzene (IPFB) can passivate the perovskite surface by forming a supra-molecular halogen bonding D-A complex (**Fig. 19a, left**).[335] They revealed that the under-coordinated iodides in perovskite thin-films tend to act as hole-trapping sites to create charge accumulation and cause undesirable charge recombination. By passivating with IPFB, the electrostatic charges of under-coordinated iodides could be shielded, thereby leading to improved PCE from 13% to over 15%. Lewis bases such as thiophene and pyridine could further be introduced to passivate the under-coordinated Pb atoms in the crystals (**Fig. 19a, right**).[336] After being passivated by Lewis bases, the non-
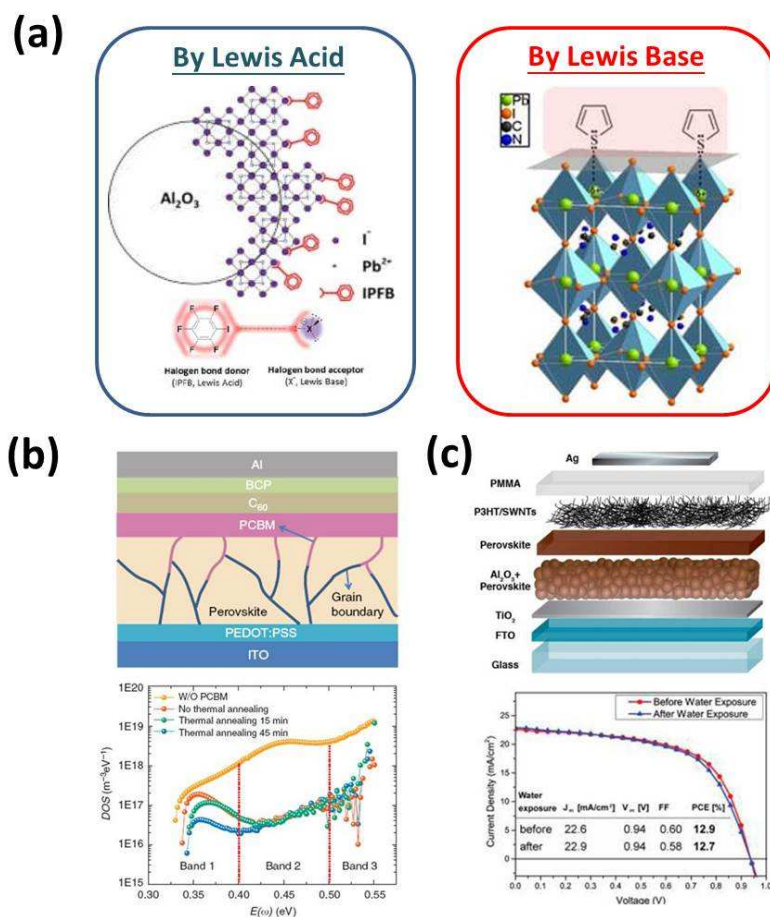

Fig. 19 (a) Passivation of perovskite surface by (left) Lewis acid and (right) Lewis based. Adapted with permission from ref. 335 & 336 Copyright 2014 American Chemical Society. (b) Device structure of perovskite/fullerene thin-film PVSC and its measured trap density of states (tDOS) by thermal admittance spectroscopy. Adapted with permission from ref. 337 Copyright 2014 Nature Publishing Group. (c) Device structures of the water-resistant PVSC and its device performance tested before and after being exposed to the running water for 60s. Adapted with permission from ref. 338 Copyright 2014 American Chemical Society.

radiative electron-hole recombination could be significantly reduced to result in a very long photoluminescence lifetime of up to $2\,\mu$s. In addition, the device performance could also be increased from 13% to 16.5%. These results suggest that the defect chemistry at perovskite interfaces plays an important role in affecting the photo-physical properties and performance of PVSC devices. More recently, Huang *et al.* also unveiled a similar passivation function by using fullerene at the perovskite/fullerene interface.[337] They pointed out that the deposition of fullerene on perovskite could efficiently reduce the charge trap states in perovskite by two orders of magnitude to simultaneously enhance device performance and alleviate hysteresis (**Fig. 19b**).

Another important concern for the perovskite interface is its thermal-/moisture-sensitive nature, which tends to deteriorate the reliability and stability of PVSCs in ambient conditions. To alleviate this problem, Snaith *et al.* have recently introduced a composite HEL comprising polymer-functionalized SWCNTs and insulating polymer matrix to enhance both the thermal stability and water-resistance of perovskite and the derived devices (**Fig. 19c**).[338] Meanwhile, Jen *et al.* have recently revealed that the ambient stability of perovskite can be improved simply by using a blade-coating technique to promote the formation of self-assembled crystalline domains at the perovskite surface, which acts like air-protection patches to retard the permeation of oxygen/moisture.[339] All these findings signify the pivotal role of interfacial engineering in improving the performance and stability of PVSCs.

8. Conclusions and Outlook

In this review, we have comprehensively surveyed the latest progress in solution-processed interfacial materials for PSCs, PTCs, and PVSCs. As revealed, diverse interfacial engineering approaches have been extensively used to enhance device efficiency and stability. Versatile solution-processable material systems have been exploited in order to meet the requirements for high-throughput manufacturing processes.

As the PCE of PSCs has exceeded the 11% milestone,[280] the development of PSCs will start to move towards dealing with relevant issues pertaining to large-scale practical applications. Therefore, accomplishing high-efficiency flexible PSCs and large-area modules will be the primary tasks in the near future.

In this regard, the development of conductive and thick charge-transporting interlayers will become a very important subject since they can provide better printing compatibility. As shown in this review, most of the organic charge-extraction layers are still restricted to having very low thickness due to their poor conductivity, which impedes future applications. Inorganic charge-extraction layers can accommodate this aspect better, however, more elaborate preparation and processing techniques are usually required. Therefore, it would be highly beneficial to develop materials that can fulfill both physical and processing needs. In addition, the development of efficient ICLs is critical for further enhancing the PCE of tandem cells. The ideal ICL should possess good solvent resistance while providing negligible electrical and/or optical losses across the sub-cells. In addition to these requirements, the development of adhesive interlayers for high-efficiency flexible PSCs is also critical for decent bending durability. Interfacial delamination in devices will deteriorate not only performance, but also stability. Given that the PCE of PVSCs is rapidly approaching 20%,[280] interfacial engineering will have an even more profound role in PVSCs. Considering its similar energy levels, charge extraction mechanism, and device structure to PSCs, principles of interfacial engineering learned from PSCs can be directly applied to PVSCs. Especially, the employment of low-temperature-processable interlayers for PVSCs will be essential for the development of high-performance flexible PVSCs. In addition, the knowledge of ICLs developed in PSCs can be used to guide the construction of perovskite-based tandem cells, including the perovskite/perovskite, perovskite/CIGS, and perovskite/Si tandem cells. It can be speculated that interfacial engineering will be one of the keys to successfully bridge these different types of sub-cells.

Owing to sensitive perovskite crystallization behavior, choosing an interlayer with proper surface energy will be very critical to enhance the crystallization kinetics and film quality of perovskites. Therefore, using interlayers to control perovskite interfaces will be an important research direction for improving understanding of relevant physical properties of perovskites, as well as realizing enhanced stability, particularly for lead-free PVSCs. In addition, it will be important to explore efficient interfacial or contact doping in PVSCs to further enhance the device performance.

Notes and references

*a*Department of Materials Science and Engineering, University of Washington, Seattle, Washington 98195-2120, USA. E-mail: ajen@u.washington.edu

*b*Department of Chemistry, University of Washington, Seattle, Washington 98195-2120, USA.

1. C. V. Hoven, A. Garcia, G. C. Bazan and T.-Q. Nguyen, *Advanced Materials*, 2008, **20**, 3793-3810.
2. A. Duarte, K.-Y. Pu, B. Liu and G. C. Bazan, *Chemistry of Materials*, 2010, **23**, 501-515.
3. F. Huang, H. Wu and Y. Cao, *Chemical Society Reviews*, 2010, **39**, 2500-2521.
4. L.-M. Chen, Z. Xu, Z. Hong and Y. Yang, *Journal of Materials Chemistry*, 2010, **20**, 2575-2598.
5. H. Ma, H.-L. Yip, F. Huang and A. K. Y. Jen, *Advanced Functional Materials*, 2010, **20**, 1371-1388.

6. R. Steim, F. R. Kogler and C. J. Brabec, *Journal of Materials Chemistry*, 2010, **20**, 2499-2512.

7. R. Po, C. Carbonera, A. Bernardi and N. Camaioni, *Energy & Environmental Science*, 2011, **4**, 285-310.

8. H.-L. Yip and A. K. Y. Jen, *Energy & Environmental Science*, 2012, **5**, 5994-6011.

9. C. Duan, K. Zhang, C. Zhong, F. Huang and Y. Cao, *Chemical Society Reviews*, 2013, **42**, 9071-9104.

10. Y.-Y. Lai, Y.-J. Cheng and C.-S. Hsu, *Energy & Environmental Science*, 2014, **7**, 1866-1883.

11. S. B. Darling and F. You, *RSC Advances*, 2013, **3**, 17633-17648.

12. A. Haugeneder, M. Neges, C. Kallinger, W. Spirkl, U. Lemmer, J. Feldmann, U. Scherf, E. Harth, A. Gügel and K. Müllen, *Physical Review B*, 1999, **59**, 15346-15351.

13. M. Theander, A. Yartsev, D. Zigmantas, V. Sundström, W. Mammo, M. R. Andersson and O. Inganäs, *Physical Review B*, 2000, **61**, 12957-12963.

14. Y.-J. Cheng, S.-H. Yang and C.-S. Hsu, *Chemical Reviews*, 2009, **109**, 5868-5923.

15. S. Günes, H. Neugebauer and N. S. Sariciftci, *Chemical Reviews*, 2007, **107**, 1324-1338.

16. F. Castet, G. D'Avino, L. Muccioli, J. Cornil and D. Beljonne, *Physical Chemistry Chemical Physics*, 2014, **16**, 20279-20290.

17. F. Gao and O. Inganas, *Physical Chemistry Chemical Physics*, 2014, **16**, 20291-20304

18. D. Wang, F. Liu, N. Yagihashi, M. Nakaya, S. Ferdous, X. Liang, A. Muramatsu, K. Nakajima and T. P. Russell, *Nano Letters*, 2014, **14**, 5727-5732.

19. J. Bisquert and G. Garcia-Belmonte, *The Journal of Physical Chemistry Letters*, 2011, **2**, 1950-1964.

20. J. Peet, J. Y. Kim, N. E. Coates, W. L. Ma, D. Moses, A. J. Heeger and G. C. Bazan, *Nat Mater*, 2007, **6**, 497-500.

21. J. K. Lee, W. L. Ma, C. J. Brabec, J. Yuen, J. S. Moon, J. Y. Kim, K. Lee, G. C. Bazan and A. J. Heeger, *Journal of the American Chemical Society*, 2008, **130**, 3619-3623.

22. C.-C. Chueh, K. Yao, H.-L. Yip, C.-Y. Chang, Y.-X. Xu, K.-S. Chen, C.-Z. Li, P. Liu, F. Huang, Y. Chen, W.-C. Chen and A. K. Y. Jen, *Energy & Environmental Science*, 2013, **6**, 3241-3248.

23. H.-C. Liao, C.-C. Ho, C.-Y. Chang, M.-H. Jao, S. B. Darling and W.-F. Su, *Materials Today*, 2013, **16**, 326-336.

24. K. Sivula, Z. T. Ball, N. Watanabe and J. M. J. Fréchet, *Advanced Materials*, 2006, **18**, 206-210.

25. J. B. Kim, K. Allen, S. J. Oh, S. Lee, M. F. Toney, Y. S. Kim, C. R. Kagan, C. Nuckolls and Y.-L. Loo, *Chemistry of Materials*, 2010, **22**, 5762-5773.

26. J.-H. Tsai, Y.-C. Lai, T. Higashihara, C.-J. Lin, M. Ueda and W.-C. Chen, *Macromolecules*, 2010, **43**, 6085-6091.

27. Z. Sun, K. Xiao, J. K. Keum, X. Yu, K. Hong, J. Browning, I. N. Ivanov, J. Chen, J. Alonzo, D. Li, B. G. Sumpter, E. A. Payzant, C. M. Rouleau and D. B. Geohegan, *Advanced Materials*, 2011, **23**, 5529-5535.

28. A. Li, J. Amonoo, B. Huang, P. K. Goldberg, A. J. McNeil and P. F. Green, *Advanced Functional Materials*, 2014, **24**, 5594-5602.

29. A. Tada, Y. Geng, Q. Wei, K. Hashimoto and K. Tajima, *Nat Mater*, 2011, **10**, 450-455.

30. B. Yang, Y. Yuan, P. Sharma, S. Poddar, R. Korlacki, S. Ducharme,

A. Gruverman, R. Saraf and J. Huang, *Advanced Materials*, 2012, **24**, 1455-1460.

31. C. J. Brabec, M. Heeney, I. McCulloch and J. Nelson, *Chemical Society Reviews*, 2011, **40**, 1185-1199.

32. A. J. Moulé and K. Meerholz, *Advanced Functional Materials*, 2009, **19**, 3028-3036.

33. P. W. M. Blom, V. D. Mihailetchi, L. J. A. Koster and D. E. Markov, *Advanced Materials*, 2007, **19**, 1551-1566.

34. S. Braun, W. R. Salaneck and M. Fahlman, *Advanced Materials*, 2009, **21**, 1450-1472.

35. W. J. Potscavage, A. Sharma and B. Kippelen, *Accounts of Chemical Research*, 2009, **42**, 1758-1767.

36. E. L. Ratcliff, B. Zacher and N. R. Armstrong, *The Journal of Physical Chemistry Letters*, 2011, **2**, 1337-1350.

37. J. Wang, C. R. Friedman, W. Cabrera, K. Tan, Y.-J. Lee, Y. J. Chabal and J. W. P. Hsu, *Journal of Materials Chemistry A*, 2014, **2**, 15288-15293.

38. C.-Z. Li, H.-L. Yip and A. K. Y. Jen, *Journal of Materials Chemistry*, 2012, **22**, 4161-4177.

39. F. C. Krebs, S. A. Gevorgyan and J. Alstrup, *Journal of Materials Chemistry*, 2009, **19**, 5442-5451.

40. F. C. Krebs, J. Fyenbo and M. Jorgensen, *Journal of Materials Chemistry*, 2010, **20**, 8994-9001.

41. F. C. Krebs, T. Tromholt and M. Jorgensen, *Nanoscale*, 2010, **2**, 873-886.

42. N. Li, D. Baran, K. Forberich, F. Machui, T. Ameri, M. Turbiez, M. Carrasco-Orozco, M. Drees, A. Facchetti, F. C. Krebs and C. J. Brabec, *Energy & Environmental Science*, 2013, **6**, 3407-3413.

43. T. R. Andersen, H. F. Dam, M. Hosel, M. Helgesen, J. E. Carle, T. T. Larsen-Olsen, S. A. Gevorgyan, J. W. Andreasen, J. Adams, N. Li, F. Machui, G. D. Spyropoulos, T. Ameri, N. Lemaitre, M. Legros, A. Scheel, D. Gaiser, K. Kreul, S. Berny, O. R. Lozman, S. Nordman, M. Valimaki, M. Vilkman, R. R. Sondergaard, M. Jorgensen, C. J. Brabec and F. C. Krebs, *Energy & Environmental Science*, 2014, **7**, 2925-2933.

44. H. Youn, T. Lee and L. J. Guo, *Energy & Environmental Science*, 2014, **7**, 2764-2770.

45. V. D. Mihailetchi, P. W. M. Blom, J. C. Hummelen and M. T. Rispens, *Journal of Applied Physics*, 2003, **94**, 6849-6854.

46. C. Tengstedt, W. Osikowicz, W. R. Salaneck, I. D. Parker, C.-H. Hsu and M. Fahlman, *Applied Physics Letters*, 2006, **88**, 053502.

47. Z. Xu, L.-M. Chen, M.-H. Chen, G. Li and Y. Yang, *Applied Physics Letters*, 2009, **95**, 013301.

48. I. Lange, J. C. Blakesley, J. Frisch, A. Vollmer, N. Koch and D. Neher, *Physical Review Letters*, 2011, **106**, 216402.

49. K. M. O'Malley, C.-Z. Li, H.-L. Yip and A. K. Y. Jen, *Advanced Energy Materials*, 2012, **2**, 82-86.

50. C.-Z. Li, C.-C. Chueh, H.-L. Yip, K. M. O'Malley, W.-C. Chen and A. K. Y. Jen, *Journal of Materials Chemistry*, 2012, **22**, 8574-8578.

51. H. Ishii, K. Sugiyama, E. Ito and K. Seki, *Advanced Materials*, 1999, **11**, 605-625.

52. S. van Reenen, S. Kouijzer, R. A. J. Janssen, M. M. Wienk and M. Kemerink, *Advanced Materials Interfaces*, 2014, **1**, 1400189.

53. R. Xia, D.-S. Leem, T. Kirchartz, S. Spencer, C. Murphy, Z. He, H. Wu, S. Su, Y. Cao, J. S. Kim, J. C. deMello, D. D. C. Bradley and J. Nelson, *Advanced Energy Materials*, 2013, **3**, 718-723.

54. B. H. Lee, I. H. Jung, H. Y. Woo, H.-K. Shim, G. Kim and K. Lee, *Advanced Functional Materials*, 2014, **24**, 1100-1108.

55. R. Kang, S.-H. Oh and D.-Y. Kim, *ACS Applied Materials & Interfaces*, 2014, **6**, 6227-6236.

56. W. E. Ford, D. Gao, N. Knorr, R. Wirtz, F. Scholz, Z. Karipidou, K. Ogasawara, S. Rosselli, V. Rodin, G. Nelles and F. von Wrochem, *ACS Nano*, 2014, **8**, 9173-9180.

57. Y. Zhou, C. Fuentes-Hernandez, J. Shim, J. Meyer, A. J. Giordano, H. Li, P. Winget, T. Papadopoulos, H. Cheun, J. Kim, M. Fenoll, A. Dindar, W. Haske, E. Najafabadi, T. M. Khan, H. Sojoudi, S. Barlow, S. Graham, J.-L. Brédas, S. R. Marder, A. Kahn and B. Kippelen, *Science*, 2012, **336**, 327-332.

58. G. Heimel, L. Romaner, J.-L. Brédas and E. Zojer, *Physical Review Letters*, 2006, **96**, 196806.

59. G. Heimel, L. Romaner, E. Zojer and J.-L. Bredas, *Accounts of Chemical Research*, 2008, **41**, 721-729.

60. H. Li, P. Paramonov and J.-L. Bredas, *Journal of Materials Chemistry*, 2010, **20**, 2630-2637.

61. J. H. Seo and T.-Q. Nguyen, *Journal of the American Chemical Society*, 2008, **130**, 10042-10043.

62. J. H. Seo, R. Yang, J. Z. Brzezinski, B. Walker, G. C. Bazan and T.-Q. Nguyen, *Advanced Materials*, 2009, **21**, 1006-1011.

63. C. Hoven, R. Yang, A. Garcia, A. J. Heeger, T.-Q. Nguyen and G. C. Bazan, *Journal of the American Chemical Society*, 2007, **129**, 10976-10977.

64. C. V. Hoven, R. Yang, A. Garcia, V. Crockett, A. J. Heeger, G. C. Bazan and T.-Q. Nguyen, *Proceedings of the National Academy of Sciences*, 2008, **105**, 12730-12735.

65. S.-I. Na, T.-S. Kim, S.-H. Oh, J. Kim, S.-S. Kim and D.-Y. Kim, *Applied Physics Letters*, 2010, **97**, 223305.

66. R. Yang, A. Garcia, D. Korystov, A. Mikhailovsky, G. C. Bazan and T.-Q. Nguyen, *Journal of the American Chemical Society*, 2006, **128**, 16532-16539.

67. A. Garcia, R. C. Bakus Ii, P. Zalar, C. V. Hoven, J. Z. Brzezinski and T.-Q. Nguyen, *Journal of the American Chemical Society*, 2011, **133**, 2492-2498.

68. J. Fang, B. H. Wallikewitz, F. Gao, G. Tu, C. Müller, G. Pace, R. H. Friend and W. T. S. Huck, *Journal of the American Chemical Society*, 2010, **133**, 683-685.

69. H.-L. Yip, S. K. Hau, N. S. Baek, H. Ma and A. K. Y. Jen, *Advanced Materials*, 2008, **20**, 2376-2382.

70. J. Park, R. Yang, C. V. Hoven, A. Garcia, D. A. Fischer, T.-Q. Nguyen, G. C. Bazan and D. M. DeLongchamp, *Advanced Materials*, 2008, **20**, 2491-2496.

71. C. Xie, L. Chen and Y. Chen, *The Journal of Physical Chemistry C*, 2013, **117**, 24804-24814.

72. X. Bulliard, S.-G. Ihn, S. Yun, Y. Kim, D. Choi, J.-Y. Choi, M. Kim, M. Sim, J.-H. Park, W. Choi and K. Cho, *Advanced Functional Materials*, 2010, **20**, 4381-4387.

73. D. Bilby, B. Frieberg, S. Kramadhati, P. Green and J. Kim, *ACS Applied Materials & Interfaces*, 2014, **6**, 14964-14974.

74. C. Waldauf, M. Morana, P. Denk, P. Schilinsky, K. Coakley, S. A. Choulis and C. J. Brabec, *Applied Physics Letters*, 2006, **89**, 233517.

75. G. Li, C.-W. Chu, V. Shrotriya, J. Huang and Y. Yang, *Applied Physics Letters*, 2006, **88**, 253503.

76. S. K. Hau, H.-L. Yip, H. Ma and A. K.-Y. Jen, *Applied Physics Letters*, 2008, **93**, 233304.

77. C.-Y. Li, T.-C. Wen, T.-H. Lee, T.-F. Guo, J.-C.-A. Huang, Y.-C. Lin and Y.-J. Hsu, *Journal of Materials Chemistry*, 2009, **19**, 1643-1647.

78. R. Søndergaard, M. Hösel, D. Angmo, T. T. Larsen-Olsen and F. C. Krebs, *Materials Today*, 2012, **15**, 36-49.

79. T. M. Clarke and J. R. Durrant, *Chemical Reviews*, 2010, **110**, 6736-6767.

80. Y. Shirota and H. Kageyama, *Chemical Reviews*, 2007, **107**, 953-1010.

81. K. Walzer, B. Maennig, M. Pfeiffer and K. Leo, *Chemical Reviews*, 2007, **107**, 1233-1271.

82. T. H. Reilly, A. W. Hains, H.-Y. Chen and B. A. Gregg, *Advanced Energy Materials*, 2012, **2**, 455-460.

83. C.-Z. Li, C.-C. Chueh, H.-L. Yip, F. Ding, X. Li and A. K. Y. Jen, *Advanced Materials*, 2013, **25**, 2457-2461.

84. C.-Z. Li, C.-C. Chueh, F. Ding, H.-L. Yip, P.-W. Liang, X. Li and A. K. Y. Jen, *Advanced Materials*, 2013, **25**, 4425-4430.

85. B. L. Schottel, H. T. Chifotides and K. R. Dunbar, *Chemical Society Reviews*, 2008, **37**, 68-83.

86. S. Guha, F. S. Goodson, L. J. Corson and S. Saha, *Journal of the American Chemical Society*, 2012, **134**, 13679-13691.

87. V. D. Mihailetchi, L. J. A. Koster, J. C. Hummelen and P. W. M. Blom, *Physical Review Letters*, 2004, **93**, 216601.

88. C. Cabanetos, A. El Labban, J. A. Bartelt, J. D. Douglas, W. R. Mateker, J. M. J. Fréchet, M. D. McGehee and P. M. Beaujuge, *Journal of the American Chemical Society*, 2013, **135**, 4656-4659.

89. L. Dou, J. You, Z. Hong, Z. Xu, G. Li, R. A. Street and Y. Yang, *Advanced Materials*, 2013, **25**, 6642-6671.

90. X. Guo, N. Zhou, S. J. Lou, J. Smith, D. B. Tice, J. W. Hennek, R. P. Ortiz, J. T. L. Navarrete, S. Li, J. Strzalka, L. X. Chen, R. P. H. Chang, A. Facchetti and T. J. Marks, *Nat Photon*, 2013, **7**, 825-833.

91. N. Camaioni and R. Po, *The Journal of Physical Chemistry Letters*, 2013, **4**, 1821-1828.

92. K. Tvingstedt, V. Andersson, F. Zhang and O. Inganäs, *Applied Physics Letters*, 2007, **91**, 123514.

93. S.-I. Na, S.-S. Kim, J. Jo, S.-H. Oh, J. Kim and D.-Y. Kim, *Advanced Functional Materials*, 2008, **18**, 3956-3963.

94. J. Y. Kim, S. H. Kim, H. H. Lee, K. Lee, W. Ma, X. Gong and A. J. Heeger, *Advanced Materials*, 2006, **18**, 572-576.

95. L. A. A. Pettersson, L. S. Roman and O. Inganäs, *Journal of Applied Physics*, 1999, **86**, 487-496.

96. J. Gilot, I. Barbu, M. M. Wienk and R. A. J. Janssen, *Applied Physics Letters*, 2007, **91**, 113520.

97. A. Hadipour, D. Cheyns, P. Heremans and B. P. Rand, *Advanced Energy Materials*, 2011, **1**, 930-935.

98. A. K. K. Kyaw, D. H. Wang, D. Wynands, J. Zhang, T.-Q. Nguyen, G. C. Bazan and A. J. Heeger, *Nano Letters*, 2013, **13**, 3796-3801.

99. H. A. Atwater and A. Polman, *Nat Mater*, 2010, **9**, 205-213.

100. M. A. Green and S. Pillai, *Nat Photon*, 2012, **6**, 130-132.

101. Q. Gan, F. J. Bartoli and Z. H. Kafafi, *Advanced Materials*, 2013, **25**, 2385-2396.

102. R. Jiang, B. Li, C. Fang and J. Wang, *Advanced Materials*, 2014, **26**, 5274-5309.

103. C.-H. Chou and F.-C. Chen, *Nanoscale*, 2014, **6**, 8444-8458.

104. D. H. Wang, D. Y. Kim, K. W. Choi, J. H. Seo, S. H. Im, J. H. Park, O. O. Park and A. J. Heeger, *Angewandte Chemie International*

Edition, 2011, **50**, 5519-5523.

105. D. H. Wang, K. H. Park, J. H. Seo, J. Seifter, J. H. Jeon, J. K. Kim, J. H. Park, O. O. Park and A. J. Heeger, *Advanced Energy Materials*, 2011, **1**, 766-770.

106. H.-C. Chen, S.-W. Chou, W.-H. Tseng, I. W. P. Chen, C.-C. Liu, C. Liu, C.-L. Liu, C.-h. Chen, C.-I. Wu and P.-T. Chou, *Advanced Functional Materials*, 2012, **22**, 3975-3984.

107. X. Li, W. C. H. Choy, H. Lu, W. E. I. Sha and A. H. P. Ho, *Advanced Functional Materials*, 2013, **23**, 2728-2735.

108. M. Salvador, B. A. MacLeod, A. Hess, A. P. Kulkarni, K. Munechika, J. I. L. Chen and D. S. Ginger, *ACS Nano*, 2012, **6**, 10024-10032.

109. B. Wu, X. Wu, C. Guan, K. Fai Tai, E. K. L. Yeow, H. Jin Fan, N. Mathews and T. C. Sum, *Nat Commun*, 2013, **4**, 2004.

110. J.-L. Wu, F.-C. Chen, Y.-S. Hsiao, F.-C. Chien, P. Chen, C.-H. Kuo, M. H. Huang and C.-S. Hsu, *ACS Nano*, 2011, **5**, 959-967.

111. J. Yang, J. You, C.-C. Chen, W.-C. Hsu, H.-r. Tan, X. W. Zhang, Z. Hong and Y. Yang, *ACS Nano*, 2011, **5**, 6210-6217.

112. L. Lu, Z. Luo, T. Xu and L. Yu, *Nano Letters*, 2012, **13**, 59-64.

113. H. Choi, S.-J. Ko, Y. Choi, P. Joo, T. Kim, B. R. Lee, J.-W. Jung, H. J. Choi, M. Cha, J.-R. Jeong, I.-W. Hwang, M. H. Song, B.-S. Kim and J. Y. Kim, *Nat Photon*, 2013, **7**, 732-738.

114. S.-W. Baek, J. Noh, C.-H. Lee, B. Kim, M.-K. Seo and J.-Y. Lee, *Sci. Rep.*, 2013, **3**, 1726.

115. S.-J. Ko, H. Choi, W. Lee, T. Kim, B. R. Lee, J.-W. Jung, J.-R. Jeong, M. H. Song, J. C. Lee, H. Y. Woo and J. Y. Kim, *Energy & Environmental Science*, 2013, **6**, 1949-1955.

116. S.-W. Baek, G. Park, J. Noh, C. Cho, C.-H. Lee, M.-K. Seo, H. Song and J.-Y. Lee, *ACS Nano*, 2014, **8**, 3302-3312.

117. H. Choi, J.-P. Lee, S.-J. Ko, J.-W. Jung, H. Park, S. Yoo, O. Park, J.-R. Jeong, S. Park and J. Y. Kim, *Nano Letters*, 2013, **13**, 2204-2208.

118. D. C. Lim, K.-D. Kim, S.-Y. Park, E. M. Hong, H. O. Seo, J. H. Lim, K. H. Lee, Y. Jeong, C. Song, E. Lee, Y. D. Kim and S. Cho, *Energy & Environmental Science*, 2012, **5**, 9803-9807.

119. B. Niesen, B. P. Rand, P. Van Dorpe, D. Cheyns, L. Tong, A. Dmitriev and P. Heremans, *Advanced Energy Materials*, 2013, **3**, 145-150.

120. J. You, X. Li, F.-x. Xie, W. E. I. Sha, J. H. W. Kwong, G. Li, W. C. H. Choy and Y. Yang, *Advanced Energy Materials*, 2012, **2**, 1203-1207.

121. X. Li, W. C. H. Choy, L. Huo, F. Xie, W. E. I. Sha, B. Ding, X. Guo, Y. Li, J. Hou, J. You and Y. Yang, *Advanced Materials*, 2012, **24**, 3046-3052.

122. X. Yang, C.-C. Chueh, C.-Z. Li, H.-L. Yip, P. Yin, H. Chen, W.-C. Chen and A. K. Y. Jen, *Advanced Energy Materials*, 2013, **3**, 666-673.

123. K. Yao, M. Salvador, C.-C. Chueh, X.-K. Xin, Y.-X. Xu, D. W. deQuilettes, T. Hu, Y. Chen, D. S. Ginger and A. K. Y. Jen, *Advanced Energy Materials*, 2014, **4**, 1400206.

124. J.-F. Salinas, H.-L. Yip, C.-C. Chueh, C.-Z. Li, J.-L. Maldonado and A. K. Y. Jen, *Advanced Materials*, 2012, **24**, 6362-6367.

125. K.-S. Chen, H.-L. Yip, J.-F. Salinas, Y.-X. Xu, C.-C. Chueh and A. K. Y. Jen, *Advanced Materials*, 2014, **26**, 3349-3354.

126. J. Zou, C.-Z. Li, C.-Y. Chang, H.-L. Yip and A. K. Y. Jen, *Advanced Materials*, 2014, **26**, 3618-3623.

127. B. O'Connor, C. Haughn, K.-H. An, K. P. Pipe and M. Shtein,

Applied Physics Letters, 2008, **93**, 223304.

128. V. J. Logeeswaran, N. P. Kobayashi, M. S. Islam, W. Wu, P. Chaturvedi, N. X. Fang, S. Y. Wang and R. S. Williams, *Nano Letters*, 2008, **9**, 178-182.

129. C.-Y. Chang, L. Zuo, H.-L. Yip, C.-Z. Li, Y. Li, C.-S. Hsu, Y.-J. Cheng, H. Chen and A. K. Y. Jen, *Advanced Energy Materials*, 2014, **4**, 1301645.

130. C.-C. Chueh, S.-C. Chien, H.-L. Yip, J. F. Salinas, C.-Z. Li, K.-S. Chen, F.-C. Chen, W.-C. Chen and A. K. Y. Jen, *Advanced Energy Materials*, 2013, **3**, 417-423.

131. K.-S. Chen, J.-F. Salinas, H.-L. Yip, L. Huo, J. Hou and A. K. Y. Jen, *Energy & Environmental Science*, 2012, **5**, 9551-9557.

132. C.-Y. Chang, L. Zuo, H.-L. Yip, Y. Li, C.-Z. Li, C.-S. Hsu, Y.-J. Cheng, H. Chen and A. K. Y. Jen, *Advanced Functional Materials*, 2013, **23**, 5084-5090.

133. L. Zuo, C.-C. Chueh, Y.-X. Xu, K.-S. Chen, Y. Zang, C.-Z. Li, H. Chen and A. K. Y. Jen, *Advanced Materials*, 2014, **26**, 6778-6784.

134. S. Y. Heriot and R. A. L. Jones, *Nat Mater*, 2005, **4**, 782-786.

135. C.-Y. Li, T.-C. Wen and T.-F. Guo, *Journal of Materials Chemistry*, 2008, **18**, 4478-4482.

136. Z. Xu, L.-M. Chen, G. Yang, C.-H. Huang, J. Hou, Y. Wu, G. Li, C.-S. Hsu and Y. Yang, *Advanced Functional Materials*, 2009, **19**, 1227-1234.

137. W. Zhang, Y. Wu, Q. Bao, F. Gao and J. Fang, *Advanced Energy Materials*, 2014, **4**, 1400359.

138. B. Meng, Y. Fu, Z. Xie, J. Liu and L. Wang, *Macromolecules*, 2014.

139. M. Jørgensen, K. Norrman and F. C. Krebs, *Solar Energy Materials and Solar Cells*, 2008, **92**, 686-714.

140. J. Huang, G. Li and Y. Yang, *Advanced Materials*, 2008, **20**, 415-419.

141. V. C. Tung, J. Kim, L. J. Cote and J. Huang, *Journal of the American Chemical Society*, 2011, **133**, 9262-9265.

142. Y.-Y. Lee, K.-H. Tu, C.-C. Yu, S.-S. Li, J.-Y. Hwang, C.-C. Lin, K.-H. Chen, L.-C. Chen, H.-L. Chen and C.-W. Chen, *ACS Nano*, 2011, **5**, 6564-6570.

143. F.-C. Chen and S.-C. Chien, *Journal of Materials Chemistry*, 2009, **19**, 6865-6869.

144. F.-C. Chen, M.-K. Chuang, S.-C. Chien, J.-H. Fang and C.-W. Chu, *Journal of Materials Chemistry*, 2011, **21**, 11378-11382.

145. S.-C. Chien, F.-C. Chen, M.-K. Chung and C.-S. Hsu, *The Journal of Physical Chemistry C*, 2011, **116**, 1354-1360.

146. J. W. Jung, J. W. Jo and W. H. Jo, *Advanced Materials*, 2011, **23**, 1782-1787.

147. Q. Tai, J. Li, Z. Liu, Z. Sun, X. Zhao and F. Yan, *Journal of Materials Chemistry*, 2011, **21**, 6848-6853.

148. Y. Shi, L. Tan, L. Chen and Y. Chen, *Journal of Materials Chemistry C*, 2014, **2**, 8054-8064.

149. L. Bian, E. Zhu, J. Tang, W. Tang and F. Zhang, *Progress in Polymer Science*, 2012, **37**, 1292-1331.

150. X. Guo, M. Baumgarten and K. Müllen, *Progress in Polymer Science*, 2013, **38**, 1832-1908.

151. M. C. Scharber and N. S. Sariciftci, *Progress in Polymer Science*, 2013, **38**, 1929-1940.

152. C.-K. Mai, H. Zhou, Y. Zhang, Z. B. Henson, T.-Q. Nguyen, A. J. Heeger and G. C. Bazan, *Angewandte Chemie International Edition*, 2013, **52**, 12874-12878.

153. H. Zhou, Y. Zhang, C.-K. Mai, S. D. Collins, T.-Q. Nguyen, G. C. Bazan and A. J. Heeger, *Advanced Materials*, 2014, **26**, 780-785.

154. J. C. Brendel, M. M. Schmidt, G. Hagen, R. Moos and M. Thelakkat, *Chemistry of Materials*, 2014, **26**, 1992-1998.

155. G. K. Mor, D. Jones, T. P. Le, Z. Shang, P. J. Weathers, M. K. B. Woltermann, K. Vakhshouri, B. P. Williams, S. A. Tohran, T. Saito, R. Verduzco, A. Salleo, M. A. Hickner and E. D. Gomez, *Advanced Energy Materials*, 2014, **4**, 1400439.

156. J. Liu, Y. Xue, Y. Gao, D. Yu, M. Durstock and L. Dai, *Advanced Materials*, 2012, **24**, 2228-2233.

157. J. Liu, M. Durstock and L. Dai, *Energy & Environmental Science*, 2014, **7**, 1297-1306.

158. S.-S. Li, K.-H. Tu, C.-C. Lin, C.-W. Chen and M. Chhowalla, *ACS Nano*, 2010, **4**, 3169-3174.

159. Y. Gao, H.-L. Yip, K.-S. Chen, K. M. O'Malley, O. Acton, Y. Sun, G. Ting, H. Chen and A. K. Y. Jen, *Advanced Materials*, 2011, **23**, 1903-1908.

160. D. R. Dreyer, S. Park, C. W. Bielawski and R. S. Ruoff, *Chemical Society Reviews*, 2010, **39**, 228-240.

161. S. Mao, H. Pu and J. Chen, *RSC Advances*, 2012, **2**, 2643-2662.

162. Y.-J. Jeon, J.-M. Yun, D.-Y. Kim, S.-I. Na and S.-S. Kim, *Solar Energy Materials and Solar Cells*, 2012, **105**, 96-102.

163. X. Liu, H. Kim and L. J. Guo, *Organic Electronics*, 2013, **14**, 591-598.

164. D. Yang, L. Zhou, L. Chen, B. Zhao, J. Zhang and C. Li, *Chemical Communications*, 2012, **48**, 8078-8080.

165. I. P. Murray, S. J. Lou, L. J. Cote, S. Loser, C. J. Kadleck, T. Xu, J. M. Szarko, B. S. Rolczynski, J. E. Johns, J. Huang, L. Yu, L. X. Chen, T. J. Marks and M. C. Hersam, *The Journal of Physical Chemistry Letters*, 2011, **2**, 3006-3012.

166. J.-M. Yun, J.-S. Yeo, J. Kim, H.-G. Jeong, D.-Y. Kim, Y.-J. Noh, S.-S. Kim, B.-C. Ku and S.-I. Na, *Advanced Materials*, 2011, **23**, 4923-4928.

167. J. Liu, Y. Xue and L. Dai, *The Journal of Physical Chemistry Letters*, 2012, **3**, 1928-1933.

168. J. Kim, V. C. Tung and J. Huang, *Advanced Energy Materials*, 2011, **1**, 1052-1057.

169. G.-Q. Fan, Q.-Q. Zhuo, J.-J. Zhu, Z.-Q. Xu, P.-P. Cheng, Y.-Q. Li, X.-H. Sun, S.-T. Lee and J.-X. Tang, *Journal of Materials Chemistry*, 2012, **22**, 15614-15619.

170. J. Liu, G.-H. Kim, Y. Xue, J. Y. Kim, J.-B. Baek, M. Durstock and L. Dai, *Advanced Materials*, 2014, **26**, 786-790.

171. J. Zou, H.-L. Yip, Y. Zhang, Y. Gao, S.-C. Chien, K. O'Malley, C.-C. Chueh, H. Chen and A. K. Y. Jen, *Advanced Functional Materials*, 2012, **22**, 2804-2811.

172. Y.-H. Chao, J.-S. Wu, C.-E. Wu, J.-F. Jheng, C.-L. Wang and C.-S. Hsu, *Advanced Energy Materials*, 2013, **3**, 1279-1285.

173. J. Meyer, S. Hamwi, M. Kröger, W. Kowalsky, T. Riedl and A. Kahn, *Advanced Materials*, 2012, **24**, 5408-5427.

174. S. Chen, J. R. Manders, S.-W. Tsang and F. So, *Journal of Materials Chemistry*, 2012, **22**, 24202-24212.

175. K. Zilberberg, J. Meyer and T. Riedl, *Journal of Materials Chemistry C*, 2013, **1**, 4796-4815.

176. K. X. Steirer, P. F. Ndione, N. E. Widjonarko, M. T. Lloyd, J. Meyer, E. L. Ratcliff, A. Kahn, N. R. Armstrong, C. J. Curtis, D. S. Ginley, J. J. Berry and D. C. Olson, *Advanced Energy Materials*, 2011, **1**, 813-820.

177. Z. Zhai, X. Huang, M. Xu, J. Yuan, J. Peng and W. Ma, *Advanced Energy Materials*, 2013, **3**, 1614-1622.

178. J. R. Manders, S.-W. Tsang, M. J. Hartel, T.-H. Lai, S. Chen, C. M. Amb, J. R. Reynolds and F. So, *Advanced Functional Materials*, 2013, **23**, 2993-3001.

179. J. Zhang, J. Wang, Y. Fu, B. Zhang and Z. Xie, *Journal of Materials Chemistry C*, 2014, **2**, 8295-8302.

180. M. Kröger, S. Hamwi, J. Meyer, T. Riedl, W. Kowalsky and A. Kahn, *Applied Physics Letters*, 2009, **95**, 123301.

181. Y.-J. Lee, J. Yi, G. F. Gao, H. Koerner, K. Park, J. Wang, K. Luo, R. A. Vaia and J. W. P. Hsu, *Advanced Energy Materials*, 2012, **2**, 1193-1197.

182. S. Murase and Y. Yang, *Advanced Materials*, 2012, **24**, 2459-2462.

183. T. Yang, M. Wang, Y. Cao, F. Huang, L. Huang, J. Peng, X. Gong, S. Z. D. Cheng and Y. Cao, *Advanced Energy Materials*, 2012, **2**, 523-527.

184. F. Xie, W. C. H. Choy, C. Wang, X. Li, S. Zhang and J. Hou, *Advanced Materials*, 2013, **25**, 2051-2055.

185. K. Zilberberg, S. Trost, H. Schmidt and T. Riedl, *Advanced Energy Materials*, 2011, **1**, 377-381.

186. K. Zilberberg, S. Trost, J. Meyer, A. Kahn, A. Behrendt, D. Lützenkirchen-Hecht, R. Frahm and T. Riedl, *Advanced Functional Materials*, 2011, **21**, 4776-4783.

187. C.-P. Chen, Y.-D. Chen and S.-C. Chuang, *Advanced Materials*, 2011, **23**, 3859-3863.

188. G. Teran-Escobar, J. Pampel, J. M. Caicedo and M. Lira-Cantu, *Energy & Environmental Science*, 2013, **6**, 3088-3098.

189. T. Stubhan, N. Li, N. A. Luechinger, S. C. Halim, G. J. Matt and C. J. Brabec, *Advanced Energy Materials*, 2012, **2**, 1433-1438.

190. H. Choi, B. Kim, M. J. Ko, D.-K. Lee, H. Kim, S. H. Kim and K. Kim, *Organic Electronics*, 2012, **13**, 959-968.

191. Z. a. Tan, L. Li, C. Cui, Y. Ding, Q. Xu, S. Li, D. Qian and Y. Li, *The Journal of Physical Chemistry C*, 2012, **116**, 18626-18632.

192. Z. a. Tan, L. Li, F. Wang, Q. Xu, S. Li, G. Sun, X. Tu, X. Hou, J. Hou and Y. Li, *Advanced Energy Materials*, 2014, **4**, 1300884.

193. F. Wang, Q. Xu, Z. a. Tan, L. Li, S. Li, X. Hou, G. Sun, X. Tu, J. Hou and Y. Li, *Journal of Materials Chemistry A*, 2014, **2**, 1318-1324.

194. Q. Xu, F. Wang, Z. a. Tan, L. Li, S. Li, X. Hou, G. Sun, X. Tu, J. Hou and Y. Li, *ACS Applied Materials & Interfaces*, 2013, **5**, 10658-10664.

195. X. Tu, F. Wang, C. Li, Z. a. Tan and Y. Li, *The Journal of Physical Chemistry C*, 2014, **118**, 9309-9317.

196. K. Wang, H. Ren, C. Yi, C. Liu, H. Wang, L. Huang, H. Zhang, A. Karim and X. Gong, *ACS Applied Materials & Interfaces*, 2013, **5**, 10325-10330.

197. X. Li, F. Xie, S. Zhang, J. Hou and W. C. H. Choy, *Advanced Functional Materials*, 2014, **24**, 7348-7356.

198. X. Zhao, C. Xu, H. Wang, F. Chen, W. Zhang, Z. Zhao, L. Chen and S. Yang, *ACS Applied Materials & Interfaces*, 2014, **6**, 4329-4337.

199. Q. Chen, B. J. Worfolk, T. C. Hauger, U. Al-Atar, K. D. Harris and J. M. Buriak, *ACS Applied Materials & Interfaces*, 2011, **3**, 3962-3970.

200. Z.-G. Zhang, B. Qi, Z. Jin, D. Chi, Z. Qi, Y. Li and J. Wang, *Energy & Environmental Science*, 2014, **7**, 1966-1973.

201. K. Sun, B. Zhao, V. Murugesan, A. Kumar, K. Zeng, J. Subbiah, W.

W. H. Wong, D. J. Jones and J. Ouyang, *Journal of Materials Chemistry*, 2012, **22**, 24155-24165.

202. H. Ye, X. Hu, Z. Jiang, D. Chen, X. Liu, H. Nie, S.-J. Su, X. Gong and Y. Cao, *Journal of Materials Chemistry A*, 2013, **1**, 3387-3394.

203. D. Chen, H. Zhou, M. Liu, W.-M. Zhao, S.-J. Su and Y. Cao, *Macromolecular Rapid Communications*, 2013, **34**, 595-603.

204. H. Wu, F. Huang, Y. Mo, W. Yang, D. Wang, J. Peng and Y. Cao, *Advanced Materials*, 2004, **16**, 1826-1830.

205. Z.-G. Zhang, H. Li, Z. Qi, Z. Jin, G. Liu, J. Hou, Y. Li and J. Wang, *Applied Physics Letters*, 2013, **102**, 143902.

206. Z.-G. Zhang, H. Li, B. Qi, D. Chi, Z. Jin, Z. Qi, J. Hou, Y. Li and J. Wang, *Journal of Materials Chemistry A*, 2013, **1**, 9624-9629.

207. S. Li, M. Lei, M. Lv, S. E. Watkins, Z. a. Tan, J. Zhu, J. Hou, X. Chen and Y. Li, *Advanced Energy Materials*, 2013, **3**, 1569-1574.

208. W. Jiao, D. Ma, M. Lv, W. Chen, H. Wang, J. Zhu, M. Lei and X. Chen, *Journal of Materials Chemistry A*, 2014, **2**, 14720-14728.

209. C. Duan, W. Cai, B. B. Y. Hsu, C. Zhong, K. Zhang, C. Liu, Z. Hu, F. Huang, G. C. Bazan, A. J. Heeger and Y. Cao, *Energy & Environmental Science*, 2013, **6**, 3022-3034.

210. C. Duan, C. Zhong, C. Liu, F. Huang and Y. Cao, *Chemistry of Materials*, 2012, **24**, 1682-1689.

211. Y.-Y. Lai, P.-I. Shih, Y.-P. Li, C.-E. Tsai, J.-S. Wu, Y.-J. Cheng and C.-S. Hsu, *ACS Applied Materials & Interfaces*, 2013, **5**, 5122-5128.

212. C. Yi, K. Yue, W.-B. Zhang, X. Lu, J. Hou, Y. Li, L. Huang, G. R. Newkome, S. Z. D. Cheng and X. Gong, *ACS Applied Materials & Interfaces*, 2014, **6**, 14189-14195.

213. Q. Mei, C. Li, X. Gong, H. Lu, E. Jin, C. Du, Z. Lu, L. Jiang, X. Meng, C. Wang and Z. Bo, *ACS Applied Materials & Interfaces*, 2013, **5**, 8076-8080.

214. X. Li, W. Zhang, Y. Wu, C. Min and J. Fang, *Journal of Materials Chemistry A*, 2013, **1**, 12413-12416.

215. Z. A. Page, Y. Liu, V. V. Duzhko, T. P. Russell and T. Emrick, *Science*, 2014, **346**, 441-444.

216. C.-Z. Li, C.-Y. Chang, Y. Zang, H.-X. Ju, C.-C. Chueh, P.-W. Liang, N. Cho, D. S. Ginger and A. K. Y. Jen, *Advanced Materials*, 2014, **26**, 6262-6267.

217. S. Woo, W. Hyun Kim, H. Kim, Y. Yi, H.-K. Lyu and Y. Kim, *Advanced Energy Materials*, 2014, **4**, 1301692.

218. Z. He, C. Zhong, S. Su, M. Xu, H. Wu and Y. Cao, *Nat Photon*, 2012, **6**, 591-595.

219. S.-H. Liao, Y.-L. Li, T.-H. Jen, Y.-S. Cheng and S.-A. Chen, *Journal of the American Chemical Society*, 2012, **134**, 14271-14274.

220. S. Liu, K. Zhang, J. Lu, J. Zhang, H.-L. Yip, F. Huang and Y. Cao, *Journal of the American Chemical Society*, 2013, **135**, 15326-15329.

221. X. Guo, M. Zhang, W. Ma, L. Ye, S. Zhang, S. Liu, H. Ade, F. Huang and J. Hou, *Advanced Materials*, 2014, **26**, 4043-4049.

222. K. Zhang, C. Zhong, S. Liu, C. Mu, Z. Li, H. Yan, F. Huang and Y. Cao, *ACS Applied Materials & Interfaces*, 2014, **6**, 10429-10435.

223. H. I. Kim, T. T. T. Bui, G.-W. Kim, G. Kang, W. S. Shin and T. Park, *ACS Applied Materials & Interfaces*, 2014, **6**, 15875-15880.

224. M. Lv, S. Li, J. J. Jasieniak, J. Hou, J. Zhu, Z. a. Tan, S. E. Watkins, Y. Li and X. Chen, *Advanced Materials*, 2013, **25**, 6889-6894.

225. Z. Tang, L. M. Andersson, Z. George, K. Vandewal, K. Tvingstedt, P. Heriksson, R. Kroon, M. R. Andersson and O. Inganäs, *Advanced Materials*, 2012, **24**, 554-558.

226. Z. Tang, W. Tress, Q. Bao, M. J. Jafari, J. Bergqvist, T. Ederth, M.

R. Andersson and O. Inganäs, *Advanced Energy Materials*, 2014, **4**, 1400643.

227. J. Sun, Y. Zhu, X. Xu, L. Lan, L. Zhang, P. Cai, J. Chen, J. Peng and Y. Cao, *The Journal of Physical Chemistry C*, 2012, **116**, 14188-14198.

228. Y. Zhu, X. Xu, L. Zhang, J. Chen and Y. Cao, *Solar Energy Materials and Solar Cells*, 2012, **97**, 83-88.

229. X. Guan, K. Zhang, F. Huang, G. C. Bazan and Y. Cao, *Advanced Functional Materials*, 2012, **22**, 2846-2854.

230. T. Yang, M. Wang, C. Duan, X. Hu, L. Huang, J. Peng, F. Huang and X. Gong, *Energy & Environmental Science*, 2012, **5**, 8208-8214.

231. C. Duan, K. Zhang, X. Guan, C. Zhong, H. Xie, F. Huang, J. Chen, J. Peng and Y. Cao, *Chemical Science*, 2013, **4**, 1298-1307.

232. B. J. Worfolk, T. C. Hauger, K. D. Harris, D. A. Rider, J. A. M. Fordyce, S. Beaupré, M. Leclerc and J. M. Buriak, *Advanced Energy Materials*, 2012, **2**, 361-368.

233. Y.-M. Chang, R. Zhu, E. Richard, C.-C. Chen, G. Li and Y. Yang, *Advanced Functional Materials*, 2012, **22**, 3284-3289.

234. J. Kesters, T. Ghoos, H. Penxten, J. Drijkoningen, T. Vangerven, D. M. Lyons, B. Verreet, T. Aernouts, L. Lutsen, D. Vanderzande, J. Manca and W. Maes, *Advanced Energy Materials*, 2013, **3**, 1180-1185.

235. F. Liu, Z. A. Page, V. V. Duzhko, T. P. Russell and T. Emrick, *Advanced Materials*, 2013, **25**, 6868-6873.

236. E. Puodziukynaite, H.-W. Wang, J. Lawrence, A. J. Wise, T. P. Russell, M. D. Barnes and T. Emrick, *Journal of the American Chemical Society*, 2014, **136**, 11043-11049.

237. S.-H. Liao, H.-J. Jhuo, Y.-S. Cheng and S.-A. Chen, *Advanced Materials*, 2013, **25**, 4766-4771.

238. J. Liu, J. Wu, S. Shao, Y. Deng, B. Meng, Z. Xie, Y. Geng, L. Wang and F. Zhang, *ACS Applied Materials & Interfaces*, 2014, **6**, 8237-8245.

239. Y. Wu, W. Zhang, X. Li, C. Min, T. Jiu, Y. Zhu, N. Dai and J. Fang, *ACS Applied Materials & Interfaces*, 2013, **5**, 10428-10432.

240. S. Qu, M. Li, L. Xie, X. Huang, J. Yang, N. Wang and S. Yang, *ACS Nano*, 2013, **7**, 4070-4081.

241. K. D. G. I. Jayawardena, R. Rhodes, K. K. Gandhi, M. R. R. Prabhath, G. D. M. R. Dabera, M. J. Beliatis, L. J. Rozanski, S. J. Henley and S. R. P. Silva, *Journal of Materials Chemistry A*, 2013, **1**, 9922-9927.

242. M. J. Beliatis, K. K. Gandhi, L. J. Rozanski, R. Rhodes, L. McCafferty, M. R. Alenezi, A. S. Alshammari, C. A. Mills, K. D. G. I. Jayawardena, S. J. Henley and S. R. P. Silva, *Advanced Materials*, 2014, **26**, 2078-2083.

243. Z. Lin, C. Jiang, C. Zhu and J. Zhang, *ACS Applied Materials & Interfaces*, 2013, **5**, 713-718.

244. C. E. Small, S. Chen, J. Subbiah, C. M. Amb, S.-W. Tsang, T.-H. Lai, J. R. Reynolds and F. So, *Nat Photon*, 2012, **6**, 115-120.

245. O. Pachoumi, C. Li, Y. Vaynzof, K. K. Banger and H. Sirringhaus, *Advanced Energy Materials*, 2013, **3**, 1428-1436.

246. B. A. MacLeod, P. Schulz, S. R. Cowan, A. Garcia, D. S. Ginley, A. Kahn and D. C. Olson, *Advanced Energy Materials*, 2014, **4**, 1400073.

247. Z. Yin, Q. Zheng, S.-C. Chen, D. Cai, L. Zhou and J. Zhang, *Advanced Energy Materials*, 2014, **4**, 1301404.

248. S. Chen, C. E. Small, C. M. Amb, J. Subbiah, T.-h. Lai, S.-W. Tsang,

J. R. Manders, J. R. Reynolds and F. So, *Advanced Energy Materials*, 2012, **2**, 1333-1337.

249. J. You, C.-C. Chen, L. Dou, S. Murase, H.-S. Duan, S. A. Hawks, T. Xu, H. J. Son, L. Yu, G. Li and Y. Yang, *Advanced Materials*, 2012, **24**, 5267-5272.

250. S. Trost, K. Zilberberg, A. Behrendt and T. Riedl, *Journal of Materials Chemistry*, 2012, **22**, 16224-16229.

251. H. Li, P. Winget and J.-L. Brédas, *Chemistry of Materials*, 2013, **26**, 631-646.

252. K. M. Knesting, H. Ju, C. W. Schlenker, A. J. Giordano, A. Garcia, O. N. L. Smith, D. C. Olson, S. R. Marder and D. S. Ginger, *The Journal of Physical Chemistry Letters*, 2013, **4**, 4038-4044.

253. C. K. Song, A. C. White, L. Zeng, B. J. Leever, M. D. Clark, J. D. Emery, S. J. Lou, A. Timalsina, L. X. Chen, M. J. Bedzyk and T. J. Marks, *ACS Applied Materials & Interfaces*, 2013, **5**, 9224-9240.

254. L. Yang, S. K. Sontag, T. W. LaJoie, W. Li, N. E. Huddleston, J. Locklin and W. You, *ACS Applied Materials & Interfaces*, 2012, **4**, 5069-5073.

255. S. K. Hau, Y.-J. Cheng, H.-L. Yip, Y. Zhang, H. Ma and A. K. Y. Jen, *ACS Applied Materials & Interfaces*, 2010, **2**, 1892-1902.

256. H. Choi, J. Lee, W. Lee, S.-J. Ko, R. Yang, J. C. Lee, H. Y. Woo, C. Yang and J. Y. Kim, *Organic Electronics*, 2013, **14**, 3138-3145.

257. S. R. Cowan, P. Schulz, A. J. Giordano, A. Garcia, B. A. MacLeod, S. R. Marder, A. Kahn, D. S. Ginley, E. L. Ratcliff and D. C. Olson, *Advanced Functional Materials*, 2014, **24**, 4671-4680.

258. Y.-S. Cheng, S.-H. Liao, Y.-L. Li and S.-A. Chen, *ACS Applied Materials & Interfaces*, 2013, **5**, 6665-6671.

259. T. Ameri, N. Li and C. J. Brabec, *Energy & Environmental Science*, 2013, **6**, 2390-2413.

260. J. You, L. Dou, Z. Hong, G. Li and Y. Yang, *Progress in Polymer Science*, 2013, **38**, 1909-1928.

261. S. W. Tong, Y. Wang, Y. Zheng, M.-F. Ng and K. P. Loh, *Advanced Functional Materials*, 2011, **21**, 4430-4435.

262. J. You, L. Dou, K. Yoshimura, T. Kato, K. Ohya, T. Moriarty, K. Emery, C.-C. Chen, J. Gao, G. Li and Y. Yang, *Nat Commun*, 2013, **4**, 1446.

263. W. Li, A. Furlan, K. H. Hendriks, M. M. Wienk and R. A. J. Janssen, *Journal of the American Chemical Society*, 2013, **135**, 5529-5532.

264. C.-C. Chen, W.-H. Chang, K. Yoshimura, K. Ohya, J. You, J. Gao, Z. Hong and Y. Yang, *Advanced Materials*, 2014, **26**, 5670-5677.

265. Y. Zhou, C. Fuentes-Hernandez, J. W. Shim, T. M. Khan and B. Kippelen, *Energy & Environmental Science*, 2012, **5**, 9827-9832.

266. A. R. bin Mohd Yusoff, S. J. Lee, H. P. Kim, F. K. Shneider, W. J. da Silva and J. Jang, *Advanced Functional Materials*, 2014, **24**, 2240-2247.

267. J.-H. Kim, C. E. Song, B. Kim, I.-N. Kang, W. S. Shin and D.-H. Hwang, *Chemistry of Materials*, 2013, **26**, 1234-1242.

268. J. W. Shim, C. Fuentes-Hernandez, Y. Zhou, A. Dindar, T. M. Khan, A. J. Giordano, H. Cheun, M. Yun, S. R. Marder and B. Kippelen, *Advanced Energy Materials*, 22014, **4**, 1400048.

269. J. Lee, H. Kang, J. Kong and K. Lee, *Advanced Energy Materials*, 2014, **4**, 1301226.

270. Y. Chen, W.-C. Lin, J. Liu and L. Dai, *Nano Letters*, 2014, **14**, 1467-1471.

271. A. Kojima, K. Teshima, Y. Shirai and T. Miyasaka, *Journal of the American Chemical Society*, 2009, **131**, 6050-6051.

272. M. M. Lee, J. Teuscher, T. Miyasaka, T. N. Murakami and H. J. Snaith, *Science*, 2012, **338**, 643-647.

273. J. Burschka, N. Pellet, S.-J. Moon, R. Humphry-Baker, P. Gao, M. K. Nazeeruddin and M. Gratzel, *Nature*, 2013, **499**, 316-319.

274. G. E. Eperon, S. D. Stranks, C. Menelaou, M. B. Johnston, L. M. Herz and H. J. Snaith, *Energy & Environmental Science*, 2014, **7**, 982-988.

275. N. Pellet, P. Gao, G. Gregori, T.-Y. Yang, M. K. Nazeeruddin, J. Maier and M. Grätzel, *Angewandte Chemie International Edition*, 2014, **53**, 3151-3157.

276. J.-W. Lee, D.-J. Seol, A.-N. Cho and N.-G. Park, *Advanced Materials*, 2014, **26**, 4991-4998.

277. N. K. Noel, S. D. Stranks, A. Abate, C. Wehrenfennig, S. Guarnera, A.-A. Haghighirad, A. Sadhanala, G. E. Eperon, S. K. Pathak, M. B. Johnston, A. Petrozza, L. M. Herz and H. J. Snaith, *Energy & Environmental Science*, 2014, **7**, 3061-3068.

278. F. Hao, C. C. Stoumpos, R. P. H. Chang and M. G. Kanatzidis, *Journal of the American Chemical Society*, 2014, **136**, 8094-8099.

279. F. Hao, C. C. Stoumpos, D. H. Cao, R. P. H. Chang and M. G. Kanatzidis, *Nat Photon*, 2014, **8**, 489-494.

280. Y. Ogomi, A. Morita, S. Tsukamoto, T. Saitho, N. Fujikawa, Q. Shen, T. Toyoda, K. Yoshino, S. S. Pandey, T. Ma and S. Hayase, *The Journal of Physical Chemistry Letters*, 2014, **5**, 1004-1011.

281. F. Zuo, S. T. Williams, P.-W. Liang, C.-C. Chueh, C.-Y. Liao and A. K. Y. Jen, *Advanced Materials*, 2014, **26**, 6454-6460.

282. J. H. Noh, S. H. Im, J. H. Heo, T. N. Mandal and S. I. Seok, *Nano Letters*, 2013, **13**, 1764-1769.

283. B. Suarez, V. Gonzalez-Pedro, T. S. Ripolles, R. S. Sanchez, L. Otero and I. Mora-Sero, *The Journal of Physical Chemistry Letters*, 2014, **5**, 1628-1635.

284. P.-W. Liang, C.-C. Chueh, X.-K. Xin, F. Zuo, S. T. Williams, C.-Y. Liao and A. K. Y. Jen, *Advanced Energy Materials*, 2015, **5**, 1400960.

285. Y. Zhao and K. Zhu, *Journal of the American Chemical Society*, 2014, **136**, 12241-12244.

286. H. Yu, F. Wang, F. Xie, W. Li, J. Chen and N. Zhao, *Advanced Functional Materials*, 2014, **24**, 7102-7108.

287. Y. Tidhar, E. Edri, H. Weissman, D. Zohar, G. Hodes, D. Cahen, B. Rybtchinski and S. Kirmayer, *Journal of the American Chemical Society*, 2014, **136**, 13249-13256.

288. S. T. Williams, F. Zuo, C.-C. Chueh, C.-Y. Liao, P.-W. Liang and A. K. Y. Jen, *ACS Nano*, 2014, **8**, 10640-10654.

289. S. D. Stranks, G. E. Eperon, G. Grancini, C. Menelaou, M. J. P. Alcocer, T. Leijtens, L. M. Herz, A. Petrozza and H. J. Snaith, *Science*, 2013, **342**, 341-344.

290. H.-S. Kim, S. H. Im and N.-G. Park, *The Journal of Physical Chemistry C*, 2014, **118**, 5615-5625.

291. J. M. Ball, M. M. Lee, A. Hey and H. J. Snaith, *Energy & Environmental Science*, 2013, **6**, 1739-1743.

292. N. J. Jeon, J. H. Noh, Y. C. Kim, W. S. Yang, S. Ryu and S. I. Seok, *Nat Mater*, 2014, **13**, 897-903.

293. K. Wojciechowski, M. Saliba, T. Leijtens, A. Abate and H. J. Snaith, *Energy & Environmental Science*, 2014, **7**, 1142-1147.

294. A. Yella, L.-P. Heiniger, P. Gao, M. K. Nazeeruddin and M. Grätzel, *Nano Letters*, 2014, **14**, 2591-2596.

295. A. Abrusci, S. D. Stranks, P. Docampo, H.-L. Yip, A. K. Y. Jen and H. J. Snaith, *Nano Letters*, 2013, **13**, 3124-3128.

296. K. Wojciechowski, S. D. Stranks, A. Abate, G. Sadoughi, A. Sadhanala, N. Kopidakis, G. Rumbles, C.-Z. Li, R. H. Friend, A. K. Y. Jen and H. J. Snaith, *ACS Nano*, 2014, **8**, 12701-12709.

297. H. J. Snaith, A. Abate, J. M. Ball, G. E. Eperon, T. Leijtens, N. K. Noel, S. D. Stranks, J. T.-W. Wang, K. Wojciechowski and W. Zhang, *The Journal of Physical Chemistry Letters*, 2014, 5, 1511-1515.

298. H.-S. Kim and N.-G. Park, *The Journal of Physical Chemistry Letters*, 2014, 5, 2927-2934.

299. S. S. Mali, C. S. Shim, H. K. Park, J. Heo and C. K. Hong, *Chemistry of Materials*, 2015, DOI: 10.1021/cm504558g.

300. Z. Zhu, J. Ma, Z. Wang, C. Mu, Z. Fan, L. Du, Y. Bai, L. Fan, H. Yan, D. L. Phillips and S. Yang, *Journal of the American Chemical Society*, 2014, **136**, 3760-3763.

301. S. K. Pathak, A. Abate, P. Ruckdeschel, B. Roose, K. C. Gödel, Y. Vaynzof, A. Santhala, S.-I. Watanabe, D. J. Hollman, N. Noel, A. Sepe, U. Wiesner, R. Friend, H. J. Snaith and U. Steiner, *Advanced Functional Materials*, 2014, **24**, 6046-6055.

302. H. Zhou, Q. Chen, G. Li, S. Luo, T.-b. Song, H.-S. Duan, Z. Hong, J. You, Y. Liu and Y. Yang, *Science*, 2014, **345**, 542-546.

303. D. Liu and T. L. Kelly, *Nat Photon*, 2014, **8**, 133-138.

304. B. J. Kim, D. H. Kim, Y.-Y. Lee, H.-W. Shin, G. S. Han, J. S. Hong, K. Mahmood, T. K. Ahn, Y.-C. Joo, K. S. Hong, N.-G. Park, S. Lee and H. S. Jung, *Energy & Environmental Science*, 2015.

305. W. H. Nguyen, C. D. Bailie, E. L. Unger and M. D. McGehee, *Journal of the American Chemical Society*, 2014, **136**, 10996-11001.

306. N. J. Jeon, H. G. Lee, Y. C. Kim, J. Seo, J. H. Noh, J. Lee and S. I. Seok, *Journal of the American Chemical Society*, 2014, **136**, 7837-7840.

307. B. Xu, E. Sheibani, P. Liu, J. Zhang, H. Tian, N. Vlachopoulos, G. Boschloo, L. Kloo, A. Hagfeldt and L. Sun, *Advanced Materials*, 2014, **26**, 6629-6634.

308. S. D. Sung, M. S. Kang, I. T. Choi, H. M. Kim, H. Kim, M. Hong, H. K. Kim and W. I. Lee, *Chemical Communications*, 2014, **50**, 14161-14163.

309. P. Qin, S. Paek, M. I. Dar, N. Pellet, J. Ko, M. Grätzel and M. K. Nazeeruddin, *Journal of the American Chemical Society*, 2014, **136**, 8516-8519.

310. J. Liu, Y. Wu, C. Qin, X. Yang, T. Yasuda, A. Islam, K. Zhang, W. Peng, W. Chen and L. Han, *Energy & Environmental Science*, 2014, **7**, 2963-2967.

311. J. H. Heo, S. H. Im, J. H. Noh, T. N. Mandal, C.-S. Lim, J. A. Chang, Y. H. Lee, H.-j. Kim, A. Sarkar, K. NazeeruddinMd, M. Gratzel and S. I. Seok, *Nat Photon*, 2013, **7**, 486-491.

312. Y. S. Kwon, J. Lim, H.-J. Yun, Y.-H. Kim and T. Park, *Energy & Environmental Science*, 2014, **7**, 1454-1460.

313. Z. Zhu, Y. Bai, H. K. H. Lee, C. Mu, T. Zhang, L. Zhang, J. Wang, H. Yan, S. K. So and S. Yang, *Advanced Functional Materials*, 2014, **24**, 7357-7365.

314. J. A. Christians, R. C. M. Fung and P. V. Kamat, *Journal of the American Chemical Society*, 2013, **136**, 758-764.

315. P. Qin, S. Tanaka, S. Ito, N. Tetreault, K. Manabe, H. Nishino, M. K. Nazeeruddin and M. Grätzel, *Nat Commun*, 2014, **5**, 3834.

316. J.-Y. Jeng, Y.-F. Chiang, M.-H. Lee, S.-R. Peng, T.-F. Guo, P. Chen and T.-C. Wen, *Advanced Materials*, 2013, **25**, 3727-3732.

317. J. You, Z. Hong, Y. Yang, Q. Chen, M. Cai, T.-B. Song, C.-C. Chen, S. Lu, Y. Liu, H. Zhou and Y. Yang, *ACS Nano*, 2014, **8**, 1674-1680.

318. O. Malinkiewicz, A. Yella, Y. H. Lee, G. M. Espallargas, M. Graetzel, M. K. Nazeeruddin and H. J. Bolink, *Nat Photon*, 2014, **8**, 128-132.

319. Z. Xiao, C. Bi, Y. Shao, Q. Dong, Q. Wang, Y. Yuan, C. Wang, Y. Gao and J. Huang, *Energy & Environmental Science*, 2014, **7**, 2619-2623.

320. P.-W. Liang, C.-Y. Liao, C.-C. Chueh, F. Zuo, S. T. Williams, X.-K. Xin, J. Lin and A. K. Y. Jen, *Advanced Materials*, 2014, **26**, 3748-3754.

321. K.-G. Lim, H.-B. Kim, J. Jeong, H. Kim, J. Y. Kim and T.-W. Lee, *Advanced Materials*, 2014, **26**, 6461-6466.

322. J.-Y. Jeng, K.-C. Chen, T.-Y. Chiang, P.-Y. Lin, T.-D. Tsai, Y.-C. Chang, T.-F. Guo, P. Chen, T.-C. Wen and Y.-J. Hsu, *Advanced Materials*, 2014, **26**, 4107-4113.

323. K.-C. Wang, J.-Y. Jeng, P.-S. Shen, Y.-C. Chang, E. W.-G. Diau, C.-H. Tsai, T.-Y. Chao, H.-C. Hsu, P.-Y. Lin, P. Chen, T.-F. Guo and T.-C. Wen, *Sci. Rep.*, 2014, **4**, 4756.

324. Z. Zhu, Y. Bai, T. Zhang, Z. Liu, X. Long, Z. Wei, Z. Wang, L. Zhang, J. Wang, F. Yan and S. Yang, *Angewandte Chemie International Edition*, 2014, **53**, 12571-12575.

325. J. H. Kim, P.-W. Liang, S. T. Williams, N. Cho, C.-C. Chueh, M. S. Glaz, D. S. Ginger and A. K. Y. Jen, *Advanced Materials*, 2015, **27**, 695-701.

326. K.-C. Wang, P.-S. Shen, M.-H. Li, S. Chen, M.-W. Lin, P. Chen and T.-F. Guo, *ACS Applied Materials & Interfaces*, 2014, **6**, 11851-11858.

327. C.-H. Chiang, Z.-L. Tseng and C.-G. Wu, *Journal of Materials Chemistry A*, 2014, **2**, 15897-15903.

328. C.-C. Chueh, C.-Y. Liao, F. Zuo, S. T. Williams, P.-W. Liang and A. K. Y. Jen, *Journal of Materials Chemistry A*, 2015, DOI:10.1039/C4TA05012F.

329. H. Zhang, H. Azimi, Y. Hou, T. Ameri, T. Przybilla, E. Spiecker, M. Kraft, U. Scherf and C. J. Brabec, *Chemistry of Materials*, 2014, **26**, 5190-5193.

330. J. Min, Z.-G. Zhang, Y. Hou, C. O. Ramirez Quiroz, T. Przybilla, C. Bronnbauer, F. Guo, K. Forberich, H. Azimi, T. Ameri, E. Spiecker, Y. Li and C. J. Brabec, *Chemistry of Materials*, 2015, **27**, 227-234.

331. K. Sun, J. Chang, F. H. Isikgor, P. Li and J. Ouyang, *Nanoscale*, 2015, **7**, 896-900.

332. Q. Xue, Z. Hu, J. Liu, J. Lin, C. Sun, Z. Chen, C. Duan, J. Wang, C. Liao, W. M. Lau, F. Huang, H.-L. Yip and Y. Cao, *Journal of Materials Chemistry A*, 2014, **2**, 19598-19603.

333. C. Roldan-Carmona, O. Malinkiewicz, A. Soriano, G. Minguez Espallargas, A. Garcia, P. Reinecke, T. Kroyer, M. I. Dar, M. K. Nazeeruddin and H. J. Bolink, *Energy & Environmental Science*, 2014, **7**, 994-997.

334. J. W. Jung, S. T. Williams and A. K. Y. Jen, *RSC Advances*, 2014, **4**, 62971-62977.

335. A. Abate, M. Saliba, D. J. Hollman, S. D. Stranks, K. Wojciechowski, R. Avolio, G. Grancini, A. Petrozza and H. J. Snaith, *Nano Letters*, 2014, **14**, 3247-3254.

336. N. K. Noel, A. Abate, S. D. Stranks, E. S. Parrott, V. M. Burlakov, A. Goriely and H. J. Snaith, *ACS Nano*, 2014, **8**, 9815-9821.

337. Y. Shao, Z. Xiao, C. Bi, Y. Yuan and J. Huang, *Nat Commun*, 22014,

5, 5784.

338. S. N. Habisreutinger, T. Leijtens, G. E. Eperon, S. D. Stranks, R. J. Nicholas and H. J. Snaith, *Nano Letters*, 2014, **14**, 5561-5568.

339. J. H. Kim, S. T. Williams, N. Cho, C.-C. Chueh and A. K. Y. Jen, *Advanced Energy Materials*, 2014, DOI:10.1002/aenm.201401229.